JOURNAL OF GEOPHYSICAL RESEARCH, VOL. 102, NO. D6, PAGES 6831–6864, MARCH 27, 1997

Radiative forcing and climate response

J. Hansen, M. Sato, and R. Ruedy

NASA Goddard Institute for Space Studies, New York

Abstract. We examine the sensitivity of a climate model to a wide range of radiative forcings, including changes of solar irradiance, atmospheric CO_2, O_3, CFCs, clouds, aerosols, surface albedo, and a "ghost" forcing introduced at arbitrary heights, latitudes, longitudes, seasons, and times of day. We show that, in general, the climate response, specifically the global mean temperature change, is sensitive to the altitude, latitude, and nature of the forcing; that is, the response to a given forcing can vary by 50% or more depending upon characteristics of the forcing other than its magnitude measured in watts per square meter. The consistency of the response among different forcings is higher, within 20% or better, for most of the globally distributed forcings suspected of influencing global mean temperature in the past century, but exceptions occur for certain changes of ozone or absorbing aerosols, for which the climate response is less well behaved. In all cases the physical basis for the variations of the response can be understood. The principal mechanisms involve alterations of lapse rate and decrease (increase) of large-scale cloud cover in layers that are preferentially heated (cooled). Although the magnitude of these effects must be model-dependent, the existence and sense of the mechanisms appear to be reasonable. Overall, we reaffirm the value of the radiative forcing concept for predicting climate response and for comparative studies of different forcings; indeed, the present results can help improve the accuracy of such analyses and define error estimates. Our results also emphasize the need for measurements having the specificity and precision needed to define poorly known forcings such as absorbing aerosols and ozone change. Available data on aerosol single scatter albedo imply that anthropogenic aerosols cause less cooling than has commonly been assumed. However, negative forcing due to the net ozone change since 1979 appears to have counterbalanced 30-50% of the positive forcing due to the increase of well-mixed greenhouse gases in the same period. As the net ozone change includes halogen- driven ozone depletion with negative radiative forcing and a tropospheric ozone increase with positive radiative forcing, it is possible that the halogen-driven ozone depletion has counterbalanced more than half of the radiative forcing due to well-mixed greenhouse gases since 1979.

1. Introduction

Global climate is complicated by the simultaneous existence of many external forcing mechanisms, as well as internal feedback processes and unforced climate variability. The Wonderland climate model, described by *Hansen et al.* [this issue] (hereinafter referred to as paper W1) is a three-dimensional general circulation model (GCM) designed to allow efficient analysis of all these mechanisms of climate change. Here we use the Wonderland model to examine how well the radiative flux change at the tropopause serves as a predictor of the climate response to different radiative forcings. This topic is of practical relevance because of the need to assess the relative climate impact of different changing atmospheric constituents. In the absence of information to the contrary, the *Intergovernmental Panel on Climate Change* (IPCC) [1990, 1994], *World Meteorological Organization* (WMO) [1992], and researchers in general have been forced to use the assumption, implicitly if not explicitly, that climate change is proportional to radiative forcing.

We described the control run of the Wonderland model with specified ocean temperatures in paper W1. Section 2 describes additional control runs, with computed sea surface temperatures, and we briefly examine how the unforced model variability is affected by fixing certain aspects of the model, such as the cloud cover. Section 3 shows the sensitivity of the model to the classical doubled CO_2 and 2% solar irradiance forcings. Section 4 illustrates that the climate model response to ozone change violates the assumption of proportionality between forcing and response. Interpretation of the model response to any forcing is

Paper number 96JD03436.

aided by section 5, which shows the model sensitivity to arbitrary "ghost" forcings introduced at different places and times, and by section 6, which shows the model sensitivity to cloud changes at arbitrary levels. Section 7 examines the model sensitivity to chlorofluorocarbon (CFC) changes, including dependence on the assumed height profile of CFC in the stratosphere. Sections 8 and 9 examine the model sensitivity to changes of aerosols and surface reflectivity.

2. Control Runs

The Wonderland model is a sector GCM with idealized geography covering 120° of longitude. The model physics and the resulting zonal mean climatology are nearly the same as the full GCM of *Hansen et al.* [1983]. The horizontal resolution is 7.83° (latitude) by 10° (longitude). The nine vertical layers include one to two layers in the stratosphere.

Control run 1, documented in paper W1, has specified sea surface temperatures. Run 1 is used to infer, from the assumption of energy conservation at each grid box, the horizontal transport of heat by the ocean, which is then used in all other control runs and in the sensitivity experiments with calculated ocean temperature. This method of specifying ocean heat transports, defined by *Russell et al.* [1985] and used by *Hansen et al.* [1984], is sometimes called the "q flux" method. In the calculation of implied ocean transports, the ocean mixed layer has a seasonally varying depth based on climatology of the real-world grid boxes indicated in Figure 2 of paper W1. The global-mean annual-maximum mixed layer depth is 107 m.

Control run 2, with calculated ocean mixed layer temperature, has a mean climate practically identical to that of run 1. However, the free ocean temperature allows greater interannual climate variability, as illustrated by the global mean surface air temperature in Figure 1. The standard deviation of the annual mean global temperature about the long-term mean is 0.13°C for run 2, for both the 200-year period (Figure 1a) and the 1000-year period (Figure 1b).

Control run 3 has diffusive mixing of temperature anomalies between the mixed layer and deeper ocean, with a stability dependent diffusion coefficient which varies from grid point to grid point as specified by *Hansen et al.* [1984]. The global ocean average of the diffusion coefficient (k) is 2.5 cm²/s (for either the whole ocean or the grid points employed in the Wonderland model), but the value of k required in a one-dimensional climate model [*Hansen et al.*, 1984] for best fit to the global mean surface temperature response of the three-dimensional model is $k \approx 1$ cm²/s. Note (Figure 1) that the diffusive mixing with the deep ocean damps surface temperature variability, so that the standard deviation of the annual mean global surface air temperature is $\sigma = 0.08$°C for run 3. The standard deviation of temperature would return to larger values if the ocean dynamical heat transports also were computed. *Manabe et al.* [1990] find $\sigma = 0.1$°C with a coupled ocean-atmosphere GCM. Detrended observations, which must also include some effect of interannual

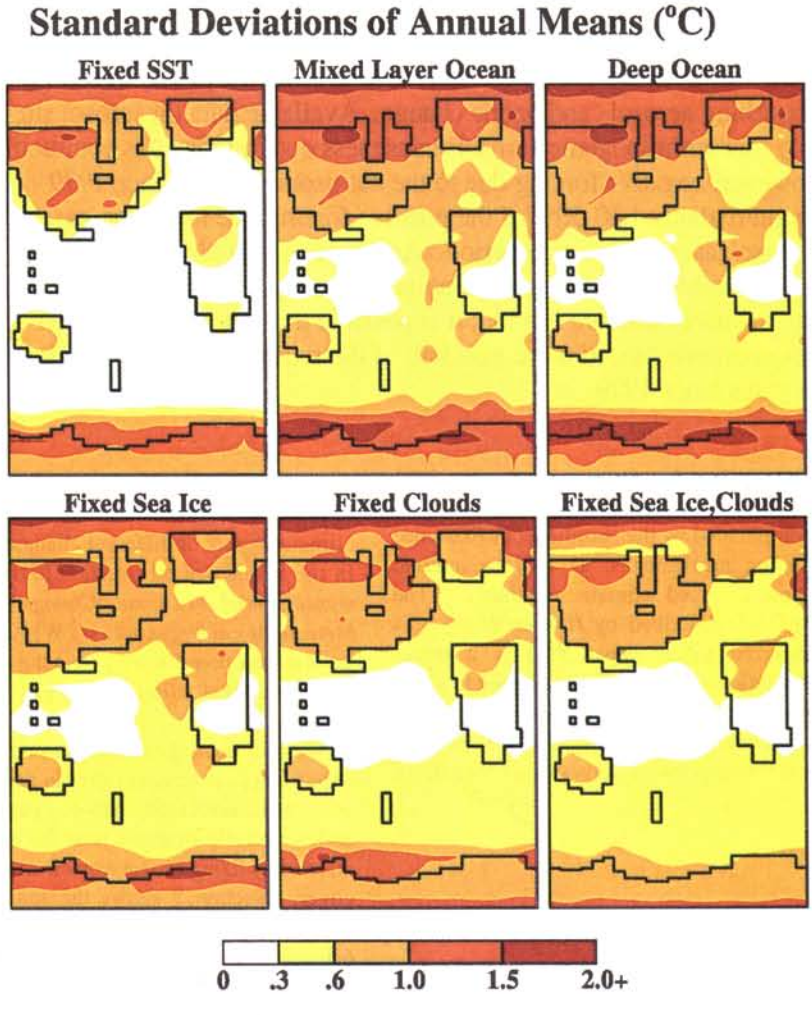

Plate 1. Standard deviation of the local annual-mean surface air temperature in first six control runs (Table 1).

variability of climate forcings, yield $\sigma = 0.1$-0.15°C [*Hansen and Lebedeff*, 1987].

We use run 2, and its variants described below, as the control runs for experiments in this paper. This is because our interest here is the equilibrium climate response to various forcings, and the mixed layer ocean approaches equilibrium rapidly. Run 3 is the control for transient climate experiments, such as those reported by *Hansen et al.* [1993a].

In variants of run 2, such as those listed in Table 1, one or more quantities (clouds, sea ice, water vapor, tropospheric lapse rate, and ground temperature) are held fixed; that is, they are not allowed to vary from year to year. One purpose of these runs is to allow the influence of certain global climate feedbacks to be studied. We do not focus on feedback studies in this paper, but the variants of run 2 help reveal the relation between radiative forcing and climate response. The values of fixed quantities are those computed at each time step and grid point in a specific year (year 217) of control run 2. Thus the weather patterns in these runs are not necessarily consistent with the geographical distributions of the specified quantities. This inconsistency should not affect the general conclusions of interest to us here.

The geographical distribution of year to year variability of surface air temperature is illustrated in Plate 1 for six control runs. Run 1 shows that there is very large interannual variability over high-latitude continental and sea ice regions even when the ocean temperature and sea ice cover are fixed. Run 2 reveals that allowing the mixed layer temperature to change increases the variability substantially over the ocean but only modestly increases variability over land. Run 3 shows that although the deep ocean heat capacity damps the variability of global mean temperature (Figure 1), it has practically no effect on the larger local variability. Thus it appears that at least with fixed ocean heat transport, the variability over land is mainly a result of fluctuating atmospheric dynamics. Although extraneous to the thesis of our present paper, this conclusion is discouraging for possible prediction of unforced interannual regional climate fluctuations. Of course, changing ocean transports, not included in the current model, may increase variability over land. For example, long-term changes of the thermohaline circulation can alter the extent of continental ice sheets, and El Nino events contribute to short-term variability. However, comparison with observed variability [*Hansen et al.*, 1996, also manuscript in preparation, 1997] suggests that unforced atmospheric fluctuations account for the larger part of interannual to decadal variability at most latitudes.

Comparison of runs 2, 2c, 2i, and 2ci reveals a positive interaction among feedback processes which increases the variability, especially an interaction between the clouds and sea ice in the region of southern hemisphere sea ice. This positive interaction, or feedback, between these two feedbacks also increases the regional and global climate sensitivity, as we show below. We do not know whether this interaction is realistically portrayed in the current model. Because cloud feedbacks are particularly uncertain, we make extensive use of the model with

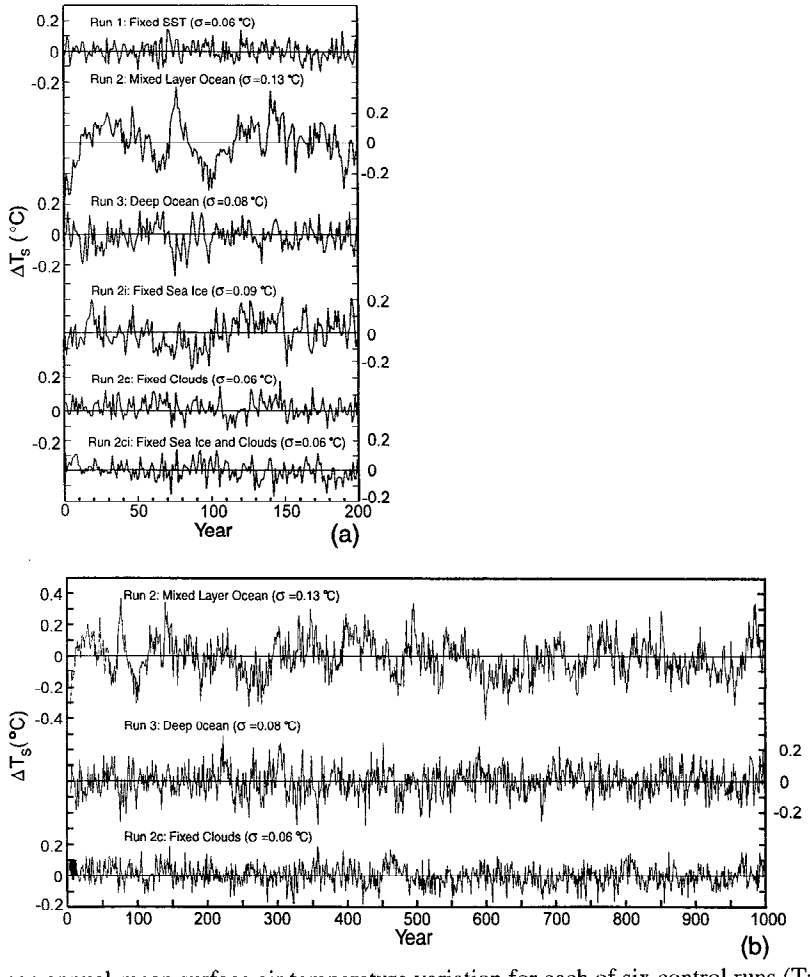

Figure 1. Global-mean annual-mean surface air temperature variation for each of six control runs (Table 1); σ is the standard deviation about the long-term mean: (a) 200 years of each run (after spin-up periods of 100 years for all runs except run 1), and (b) 1000 years of the three long runs.

Table 1. Wonderland Model Control Runs

Run	Years	Experiment Description
1	100	specified SST; generates implied ocean transports
2	1300	mixed layer ocean with specified heat transports
3	1000	same as run 2, but diffusive heat mixing with deep ocean
2c	1000	same as run 2, but clouds fixed
2i	300	same as run 2, but sea ice fixed
2ci	300	same as run 2, but clouds and sea ice fixed
2ciql	20	same as run 2ci, but water vapor and lapse rate fixed
2ciqlg	3	same as run 2ciql, but ground temperature fixed

Runs 2ciql and 2ciqlg are the control runs for calculation of ΔT_0 and F_a, respectively.

fixed clouds, as well as the standard model in which all feedbacks are allowed to operate. Note that fixing the clouds reduces variability in the tropics, as well as at high latitudes.

Control run 2ciql has the clouds, sea ice, atmospheric water vapor, and tropospheric lapse rate all held fixed. Thus when a radiative perturbation is inserted into this model, comparison to control run 2ciql yields the surface temperature change in the absence of feedbacks, ΔT_0. This ΔT_0 is the three-dimensional model equivalent of ΔT_0 defined by *Hansen et al.* [1984] for a one-dimensional (1-D) radiative-convective model. The values of ΔT_0 computed with the three-dimensional (3-D) and 1-D models are generally similar, but the 3-D model should give a more realistic global average, especially for forcings which are not globally distributed.

Control run 2ciqlg fixes, in addition, the ground temperature, so that only stratospheric temperature is allowed to adjust. Thus when a radiative perturbation is inserted into this model the radiative flux change at the tropopause or at the top of the atmosphere, after a one year spin-up, is the 3-D adjusted radiative forcing. Our 3-D adjusted forcing is equivalent to the 2-D adjusted forcings of *IPCC* [1990, 1992], *Ramaswamy et al.* [1992], and *Schwarzkopf and Ramaswamy* [1993], except that our result allows the possibility of effects due to stratospheric dynamical changes.

The lengths of the control runs are given in Table 1. In the following sections the experiment runs use the mixed layer ocean (control run 2) and are generally 100 years in length, with the equilibrium response taken to be the mean for years 41-100.

3. CO_2 and Solar Irradiance Experiments

We first discuss radiative forcings in general (section 3.1) and the $2\times CO_2$ and spectrally uniform +2% S_0 forcings in particular (section 3.2). We then examine the climate model response to these two idealized forcings (section 3.3), and the model response to spectrally and temporally varying forcings related to the solar cycle (section 3.4).

3.1. Radiative Forcing Discussion

A radiative forcing is a change imposed on the planetary radiation balance. It is measured by the net radiative flux change, at some level in the atmosphere, calculated to occur in response to the perturbation, which may be a change of incident solar radiation, atmospheric composition, or planetary surface properties, for example. Several quantitative definitions of radiative forcing are in use, their differences depending upon the atmospheric level at which the flux change is computed and upon whether the stratospheric temperature profile is allowed to adjust to the perturbation.

The simplest useful definition of radiative forcing is the instantaneous flux change at the tropopause. This is easy to compute because it does not require iterations. This forcing is called "mode A" by *WMO* [1992]. We refer to this forcing as the "instantaneous forcing", F_i, using the nomenclature of *Hansen et al.* [1993c]. In a less meaningful alternative, F_i is computed at the top of the atmosphere; we include calculations of this alternative for $2\times CO_2$ and +2% S_0 for the sake of comparison (Table 2).

An improved measure of radiative forcing is obtained by allowing the stratospheric temperature to adjust to the presence of the perturber, to a radiative equilibrium profile, with the tropospheric temperature held fixed. This forcing is called "mode B" by *WMO* [1992]; we refer to it here as the "adjusted forcing", F_a [*Hansen et al.*, 1993c]. The rationale for using the adjusted forcing is that the radiative relaxation time of the stratosphere is only several months [*Manabe and Strickler*, 1964], compared to several decades for the troposphere [*Hansen*

Table 2. The $2\times CO_2$ and $\pm 2\%$ S_0 Experiments: Global Instantaneous and Adjusted Radiative Forcings and Equilibrium Responses

	F_i[a], W/m²				ΔT_s, °C		$\Delta T_s/F_a$		R	
Experiment	TOA	Trop	F_a, W/m²	ΔT_0, °C	Fixed Clouds	All Feedbacks	Fixed Clouds	All Feedbacks	Fixed Clouds	All Feedbacks
$2\times CO_2$	2.62	4.75	4.19	1.24	2.88	3.84	0.69	0.92	1.07	1.26
$+2\%S_0$	4.67	4.39	4.48	1.33	2.88	3.22	0.64	0.72	1.00	1.00
$-2\%S_0$	-4.67	-4.39	-4.48	-1.33	-3.05	-4.70	0.68	1.05	1.00	1.00

[a] The instantaneous flux changes are shown at the top of the atmosphere (TOA) and the tropopause, with the latter value being the more meaningful climate forcing.

et al., 1985], and thus the adjusted forcing should be a better measure of the expected climate response for forcings which are present at least several months. This expectation tends to be borne out by our Wonderland simulations.

The adjusted forcing can be calculated at the top of the atmosphere because the net radiative flux is constant throughout the stratosphere in radiative equilibrium. The calculated F_a depends on where the tropopause level is specified. We specify this level as 100 mbar from the equator to 40° latitude, changing to 189 mbar there, and then increasing linearly to 300 mbar at the poles. We calculate flux changes twice, letting the fixed lapse rate region extend to the discrete GCM levels just below and just above this specified tropopause level, and then interpolate to obtain F_a at this specified level. Although the specified tropopause level is somewhat arbitrary, we have verified that the conclusions in this paper are not altered qualitatively by the precise level selected.

We anticipate that investigators will continue to use different choices for the radiative forcing (instantaneous or adjusted) and the level at which it is calculated. Thus we provide values for alternative choices, which may aid comparisons among different investigators provided that they define their choice of forcing and atmospheric level. However, we caution that quantitative variations in computed forcings will also be caused by differing approximations in radiative calculations, differing methods of averaging in 1-D, 2-D, and 3-D models, and other such factors.

Finally, the cartoons in Figure 2 illustrate the differences among the instantaneous forcing (F_i), the adjusted forcing (F_a), the no-feedback surface temperature response (ΔT_0), and the equilibrium response (ΔT_s). It is apparent that one might anticipate F_a and ΔT_0 to differ only by a scale factor, and indeed, we usually find ΔT_0(°C) ~ 0.3 F_a(W/m²). *IPCC* [1994] takes this empirical proportionality between F_a and ΔT_0 as an indication that F_a is an adequate measure of the expected climate response. However, F_a and ΔT_0 are simply different expressions of the same physical assumption, specifically, that the lapse rate in the troposphere is fixed and the lapse rate in the stratosphere is determined by radiative equilibrium. The real issue is whether ΔT_s, the surface temperature change, is proportional to F_a when the tropospheric lapse rate is allowed to change in response to climate feedbacks including cloud changes (Figure 2d).

3.2. The 2×CO_2 and Spectrally Uniform +2% S_0 Forcings

The 2×CO_2 and +2% S_0 forcings are used in Figure 3, in an elaboration of a cartoon used to illustrate the Earth's greenhouse effect and the expected radiative-convective response to these two forcings [*Hansen et al.*, 1993a]. The Earth absorbs about 240 W/m² of solar energy and, on average, must radiate that amount of thermal energy back to space. The effective radiating temperature required to yield that outgoing flux is 255°K (-18°C), which is the temperature at the mean level of emission to space at about 6 km altitude. The mean tropospheric temperature gradient is about 5.5°C/km, so the surface temperature is about 33°C warmer than it would be if the atmosphere were transparent (and the planetary albedo were still 0.3).

If solar irradiance increases 2% (at all wavelengths), the instantaneous flux change at the top of the atmosphere is 4.7 W/m². However, a fraction of this energy is absorbed in the stratosphere, which is not well coupled by atmospheric motions to the troposphere, so much of the stratospherically absorbed solar radiation is radiated back to space without affecting the surface temperature. Thus the instantaneous flux change at the tropopause, which is about 4.4 W/m², is a better measure of the forcing of surface temperature. The adjusted forcing, Table 2, is close in value to the instantaneous forcing at the tropopause, because the stratospheric temperature change is small. In order for the planet to radiate 4.5 W/m² more energy back to space, thus restoring energy balance, the surface would need to warm about 1.3°C (ΔT_0) if the atmospheric temperature gradient and all other factors were fixed.

If the amount of CO_2 in the air is doubled, the atmosphere becomes more opaque, temporarily reducing thermal emission to space. The instantaneous flux change at the tropopause is about 4.7 W/m², but the flux change at the top of the atmosphere is only about 2.6 W/m², because the added CO_2 helps the stratosphere radiate to space more efficiently. The flux change at the tropopause is more relevant to the expected surface temperature change, as shown by comparison to the adjusted forcing, which is about 4.2 W/m². Thus the 2×CO_2 forcing is almost as large as for +2% S_0, and in both cases the expected

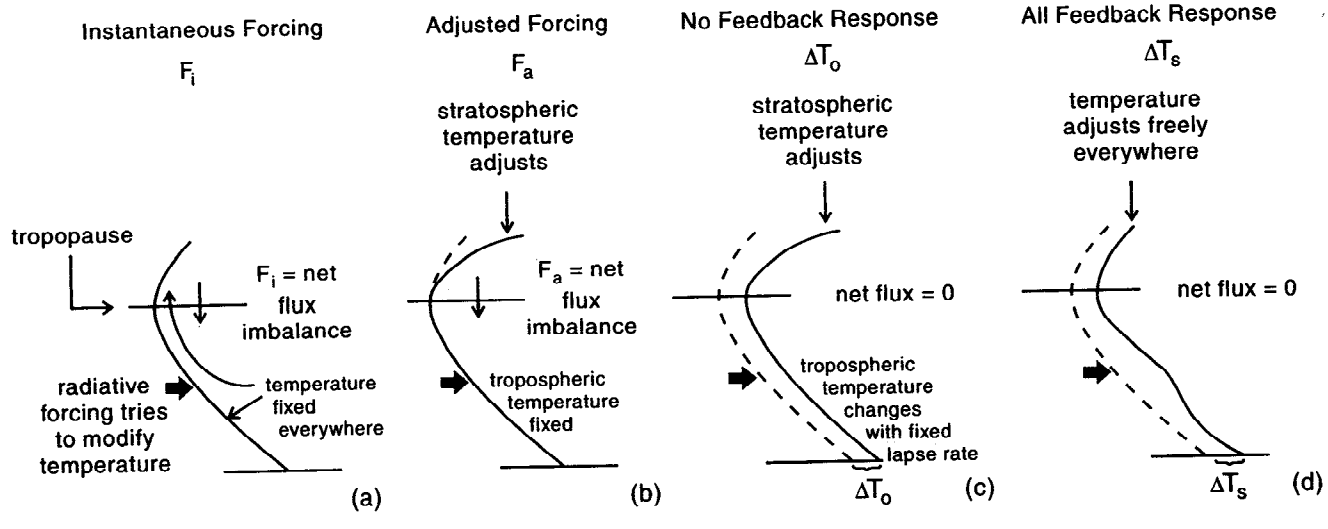

Figure 2. Cartoon showing the assumptions used in calculating (a) F_i, the instantaneous radiative forcing, (b) F_a, the adjusted radiative forcing, (c) ΔT_0, the no-feedback surface temperature response to a radiative forcing, and (d) ΔT_s, the surface air temperature response including climate feedback effects.

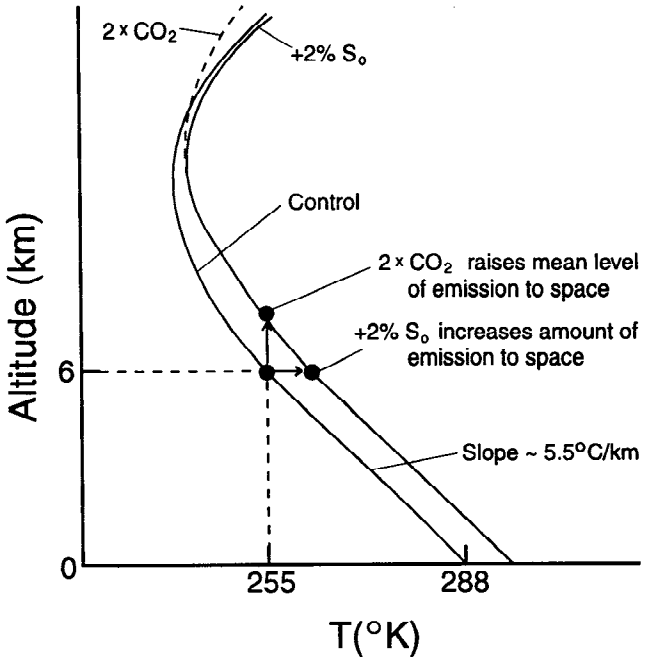

Figure 3. Cartoon of global mean greenhouse effect and alterations by radiative forcings. A solar irradiance increase of 2% increases the energy absorbed by the troposphere about 4.5 W/m^2. Doubling of atmospheric CO_2 decreases thermal emission to space almost the same amount after the stratospheric temperature has adjusted. In either case the tropospheric temperature must rise by about 1.2-1.3°C to restore planetary energy balance if the tropospheric lapse rate and other climate feedbacks are not allowed to change. The temperature profile is schematic and ΔT is exaggerated; the temperature minimum and the level at which the CO_2 effect switches from warming to cooling both occur in the 15-18 km range.

surface temperature change in the absence of climate feedbacks is $\Delta T_0 \sim 1.2$-1.3°C.

However, the quantity of most interest is ΔT_s, the surface temperature response when climate feedbacks are allowed to operate. The classical 2×CO_2 and 2% solar irradiance GCM experiments of *Manabe and Wetherald* [1975] and *Wetherald and Manabe* [1975] yielded global mean $\Delta T_s \sim 3$°C for either forcing. Later GCM investigations also found similar climate model responses to these two forcings, but the magnitude of the response differed from one climate model to another. These results were widely interpreted as indicating that although climate feedbacks and thus climate sensitivity differ from model to model, climate response is proportional to the radiative forcing. Therefore researchers in general and the Intergovernmental Panel on Climate Change [*IPCC*, 1990, 1994], in considering possible climate effects of anthropogenic activities, have used the radiative forcing as a measure of the expected climate response.

The assumption that the climate forcing and response are proportional is a useful approximation, which for practical considerations must be widely used, but for this reason it is important to have a good understanding of its basis and to determine whether there are situations where inaccuracies are sufficient to warrant identification. For these purposes it seems appropriate to study first the classical 2×CO_2 and 2% S_0 forcings.

3.3. GCM Response to 2×CO_2 and 2% S_0 Forcings

We reconsider the 2×CO_2 and (spectrally uniform) 2% solar irradiance forcings, thus calibrating the climate sensitivity of our present model and providing a precise comparison of the different definitions of radiative forcing. Our control runs have solar irradiance 1368 W/m^2, planetary albedo 32%, and absorbed solar energy about 233 W/m^2. The instantaneous forcing at the top of the atmosphere is thus about 4.66 W/m^2 for a 2% solar irradiance change. The control runs have a CO_2 amount of 285 ppm, appropriate for 1850. The accuracy of the radiative transfer calculations for CO_2 change has been tested by comparison with line-by-line calculations [*Cess et al.*, 1993]; the GCM parameterization was found to yield a forcing about 5% less than the line-by-line results, probably because of the omission of some weak lines in the GCM calculations.

We note that the climate sensitivity of the Wonderland model is somewhat less than that of the parent model II [*Hansen et al.*, 1983], which had a global mean surface air warming of 4.2°C for 2×CO_2 [*Hansen et al.*, 1984]. This is because of the small alteration in global cloud feedbacks (appendix of paper W1) which results in a more moderate net positive cloud feedback. We note also that the model's sensitivity is higher in the direction of colder climates; this characteristic, in common with other models and presumably with the real world, arises because of the larger sea ice feedback in the colder climate.

Plates 2 and 3 and Table 2 summarize the instantaneous forcing, adjusted forcing, and equilibrium response of the Wonderland model for the 2×CO_2 and 2% S_0 experiments. The equilibrium response is shown for both the fixed cloud and standard (all feedbacks) models. In Table 2 we include results for decreased solar irradiance (-2% S_0) to illustrate quantitatively the higher climate sensitivity toward colder climates. This variation of sensitivity with the mean climate state should be borne in mind when comparing the responses for forcings of different magnitudes and/or forcings of opposite sign.

The zonal mean radiative forcings and equilibrium responses are summarized in Figure 4. It can be seen that for CO_2 and S_0 forcings the tropospheric temperature change is reasonably constant with altitude, consistent with the fixed lapse rate assumption used in most radiative-convective climate models.

The responses to these comparable global forcings, 2×CO_2 and +2% S_0, are similar in a gross sense, as found by previous investigators. However, as we show in the sections below, the similarity of the responses is partly accidental, a cancellation of two contrary effects. We show in section 5 that the climate model (and presumably the real world) is much more sensitive to a forcing at high latitudes than to a forcing at low latitudes; this tends to cause a greater response for 2×CO_2 (compare Figures 4c and 4g); but the model is also more sensitive to a forcing that acts at the surface and lower troposphere than to a forcing which acts higher in the troposphere; this favors the solar forcing (compare Figures 4a and 4e), partially offsetting the latitudinal sensitivity.

It is useful to define a number measuring the effectiveness of any climate forcing for altering surface temperature. We take the climate sensitivity to a spectrally uniform change of solar irradiance (perhaps the simplest global climate forcing) as a standard for comparison. That is, for an arbitrary forcing, define a responsivity

$$R\ (\text{arbitrary forcing}) = \frac{\Delta T_s\ (\text{arbitrary forcing})}{\Delta T_s\ (\Delta S_0\ \text{forcing})},$$

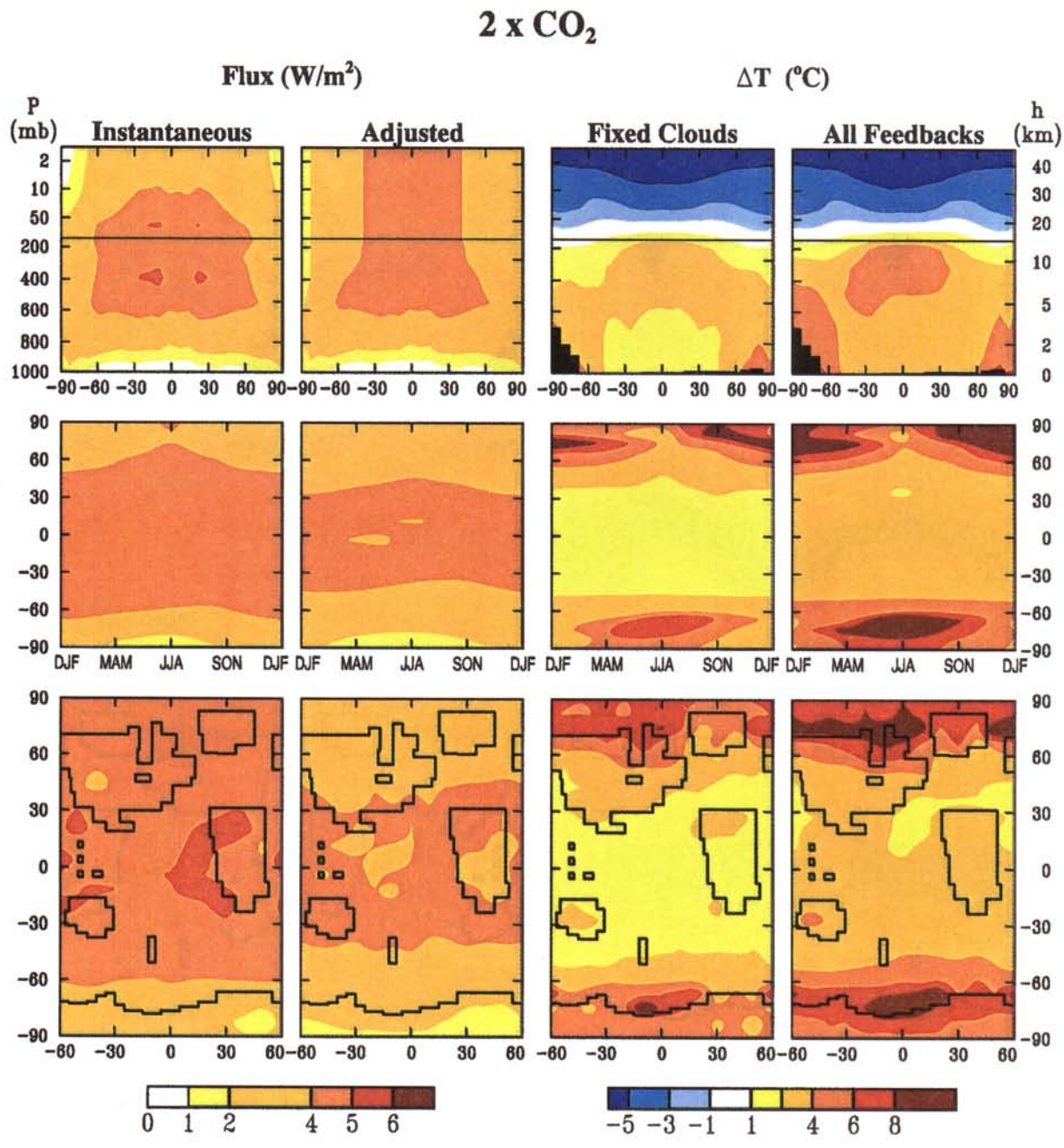

Plate 2. Forcings and responses in $2\times CO_2$ experiments with the Wonderland model, specifically the instantaneous and adjusted radiative flux changes and the equilibrium temperature changes for the fixed cloud and standard (all feedbacks) versions of the Wonderland model. (top) The radiative forcings and equilibrium temperature responses as a function of both pressure (left scale) and height (right scale), with latitude on the horizontal scale. (middle) The forcings and surface air temperature response versus latitude and season. (bottom) The geographical distribution of forcings and response.

with the two ΔT_s calculated for the same adjusted forcing, F_a. R is unity for a forcing equally as effective as solar irradiance change. R should be near unity for all forcings if the adjusted forcing is a good predictor of climate response.

We have calculated $\Delta T_s(\Delta S_0)$ only for $\Delta S_0 = \pm 2\%$ (Table 2), corresponding to $F_a = \pm 4.48$ W/m². Intermediate values are obtained from the quadratic fits

Fixed clouds $\Delta T_s = -0.0042\, F_a^2 + 0.66\, F_a$

All feedbacks $\Delta T_s = -0.0369\, F_a^2 + 0.88 F_a$.

These relations are expected to be accurate only for $|F_a| \leq 5$ W/m². Values given for R are limited in precision by unforced variability in the finite runs of the GCM. We estimate the typical uncertainty of R as ±0.02.

Our present results indicate that CO_2 is more effective than an equivalent spectrally uniform change of S_0. Specifically, $R(2\times CO_2) = 1.07$ for fixed clouds and $R(2\times CO_2) = 1.26$ for calculated clouds. Thus, although there is partial cancellation of two effects discussed above, the greater high-latitude forcing by CO_2 is the larger effect and yields a greater global mean

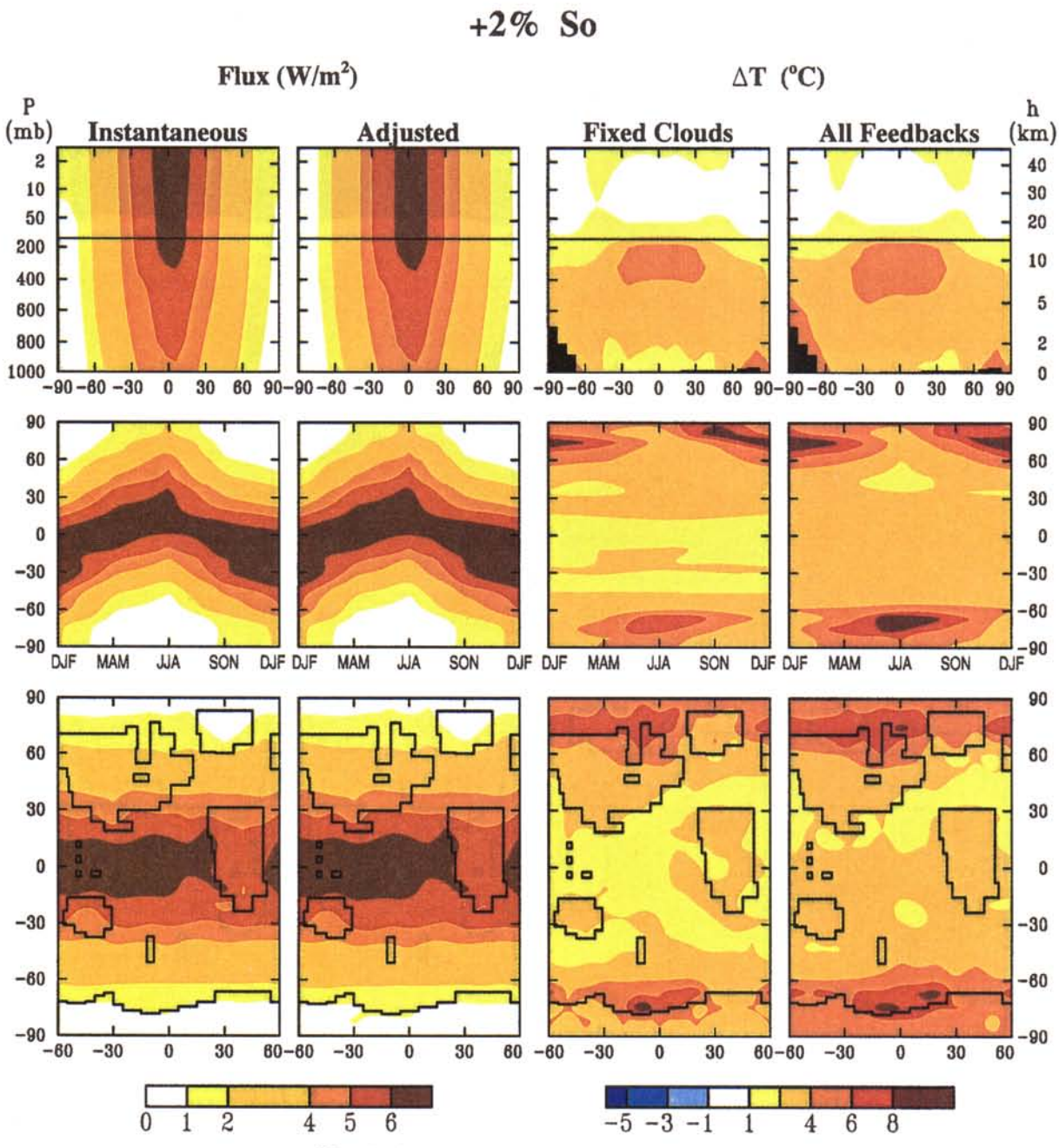

Plate 3. Same as Plate 2, but for +2% S_0 experiments.

response. The greater sensitivity to CO_2 with calculated clouds is largely a result of the positive interaction between sea ice changes and cloud changes, which is eliminated with fixed clouds. Although we suspect that the positive interaction between sea ice and cloud changes in our calculated cloud model is excessive, we cannot determine which model version is more realistic. Nevertheless, these results illustrate the absence of exact equivalency of different forcings, even for S_0 and CO_2 changes.

3.4. Climate Forcings Related to Solar Cycle

In this section we consider temporally varying and spectrally varying changes of S_0. Plate 4 shows the amplitude of the surface air temperature response for sinusoidally varying solar irradiance of period 10 years and amplitude $\Delta S_0 = 1\%$ (range $\Delta S_0 = 2\%$). These are obtained as the average of the last twenty 10-year periods in 250-year runs of the Wonderland model.

The response to an approximately 10-year periodic forcing has relevance to the real world, as evidence of a solar cycle signal has been detected in surface air temperatures [*Currie*, 1981; *Stevens and North*, 1996]. In principle, if the amplitude of ΔS_0 were known, climate sensitivity could be inferred from measured changes of surface air temperature, but the mean amplitude of 0.37-0.39°C (about twice that much in some land regions) in Plate 4 corresponds to only about 0.01°C (0.02°C in some land regions) for the 0.05% mean range of solar cycle variability assumed by *Stevens and North* [1996] for the past century.

Comprehensive analysis of the implications for climate sensitivity of calculated climate variations over the solar cycle is

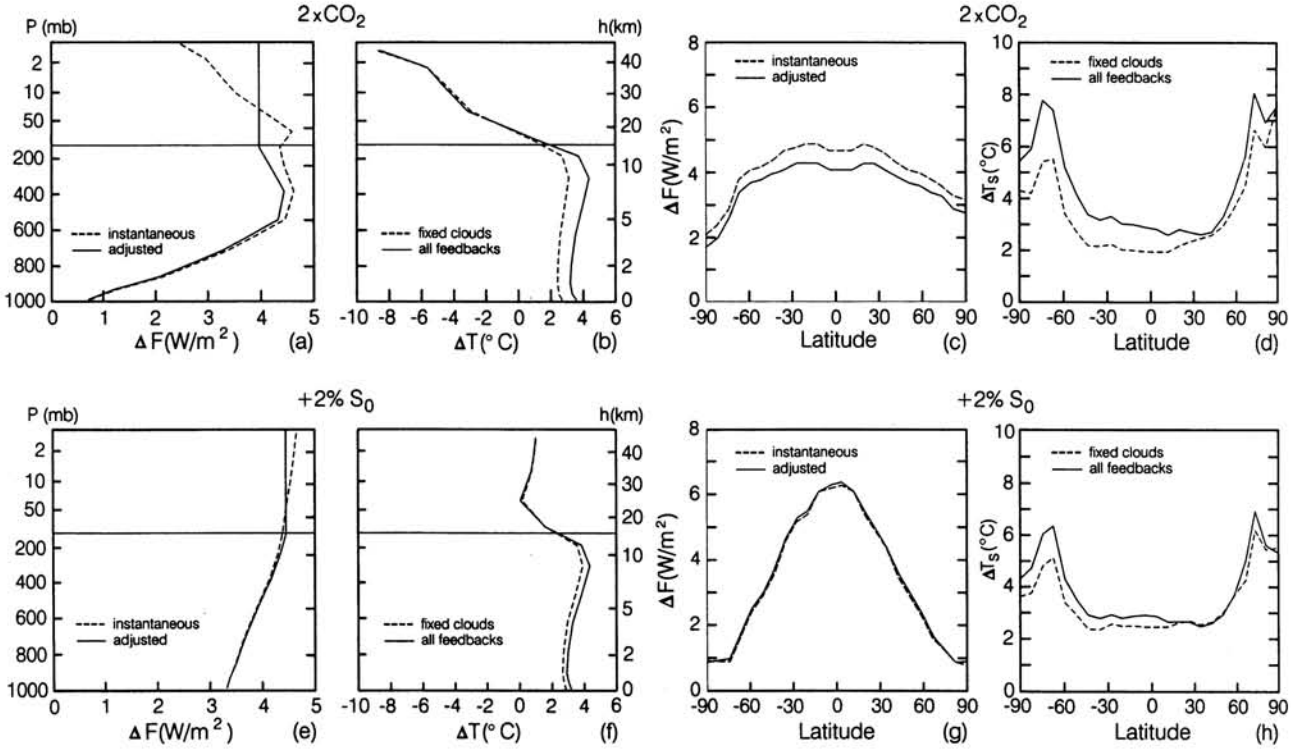

Figure 4. Forcings and responses in $2\times CO_2$ and +2% S_0 experiments. Figures 4a and 4e are the altitude distributions of the net radiative flux. Figures 4b and 4f are the altitude distribution of equilibrium temperature change. Figures 4c and 4g are the zonal mean forcing versus latitude. Figures 4d and 4h are the zonal mean surface temperature response.

beyond the scope of this paper. However, two conclusions are apparent from Plate 4.

First, the amplitude of the surface air temperature response to the climate forcing is affected little by mixing of the heat perturbation into the deep ocean, specifically the global mean amplitude of the ΔT_s response is reduced from 0.388°C to 0.381°C by inclusion of the full ocean in the model. By itself, this result would be encouraging for empirical studies of climate sensitivity, because it implies that it is only necessary that the model used for interpretation of observed data employ the proper

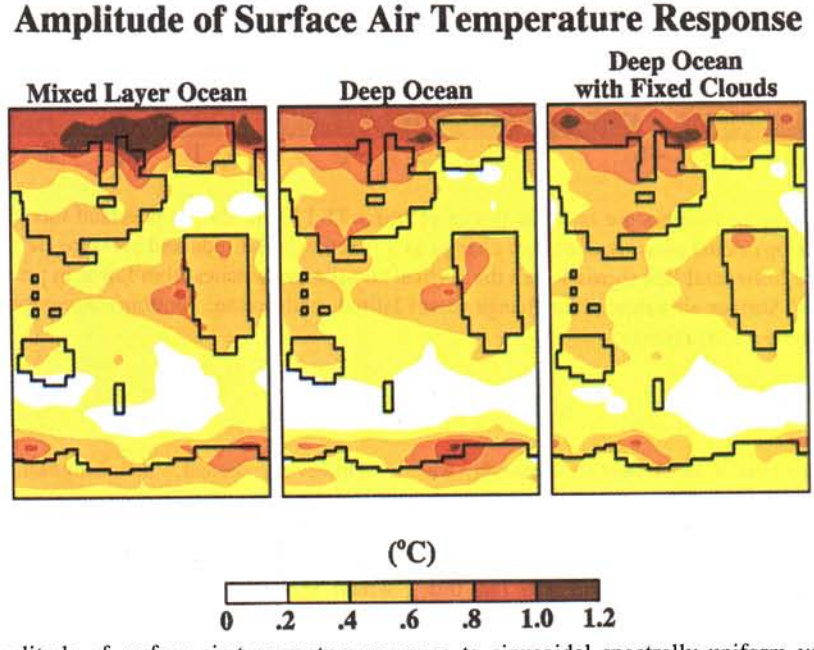

Plate 4. Amplitude of surface air temperature response to sinusoidal spectrally uniform variation of solar irradiance with period 10 years and amplitude $\Delta S_0 = 1\%$. Results are a smoothed 10-year response obtained by averaging the last twenty 10-year periods in 250 year runs of the Wonderland model. Amplitudes of the global mean response for these three cases are (a) 0.388°C, (b) 0.381°C, and (c) 0.377°C.

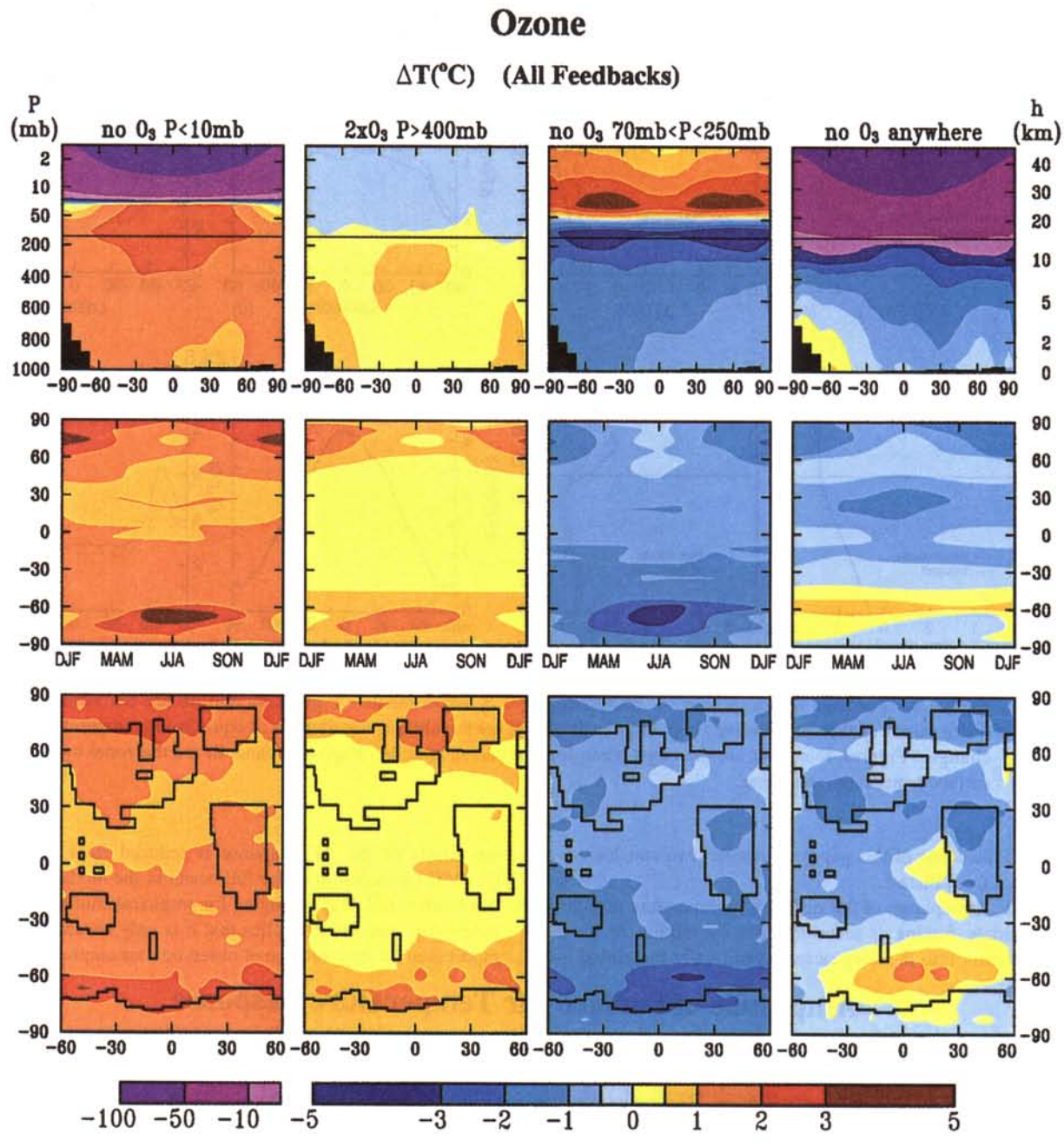

Plate 5. Equilibrium temperature changes (mean of years 71-130) in the Wonderland model for four ozone experiments. (top) Zonal mean temperature change as a function of latitude and pressure (left scale) or height (right scale); the horizontal line shows where the vertical coordinate switches from linear in pressure to linear in height. (middle) Surface air temperature change versus latitude and season. (bottom) Geographical distribution of surface air temperature change.

(annual maximum) ocean mixed layer depth. However, we caution that this conclusion is based on an ocean model which crudely represents heat perturbations as a passive diffusive tracer. Empirical evidence for the surface temperature response after large volcanoes [*Hansen et al.*, 1996] suggests that this approximation may understate the rate of heat exchange with the deeper ocean, which means that the actual response to the solar cycle may be damped even somewhat more than in the present model.

However, second, the immeasurably small difference (0.004°C) in the calculated surface air temperature response for models differing by about one quarter in their equilibrium climate sensitivities (Plater 4b and 4c) indicates how difficult it would be to usefully infer climate sensitivity from temperature changes observed over the solar cycle. This result is consistent with the relation between climate sensitivity and the response time to a forcing [*Hansen et al.*, 1985], which shows that 10 years is short compared to the equilibrium response time. We

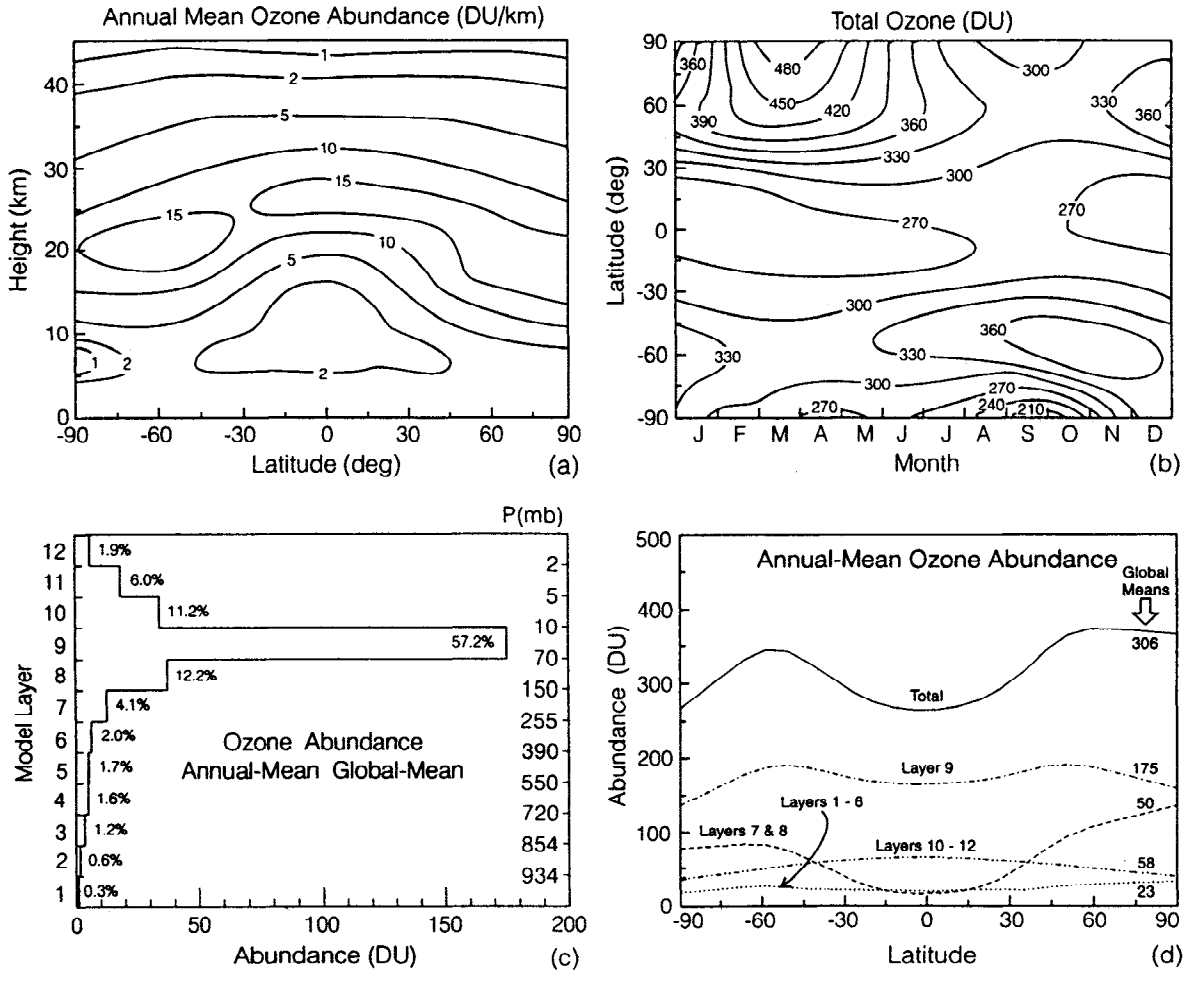

Figure 5. Ozone abundance in our GCM control runs, based on work by *McPeters et al.* [1993]. The ozone amount is independent of longitude. Layers 1-9 are the layers of the GCM below 10 mbar, in which atmospheric dynamics is computed; the three layers above the 10 mbar level interact radiatively with the atmosphere below [cf. *Hansen et al.*, 1983]. The presentations emphasize ozone variation with (a) height, (b) season, (c) model layer, and (d) latitude.

conclude that it will not be possible to infer climate sensitivity from observed response to a small forcing with such a short period. At best, a measured response to solar irradiance variability can be used to set a lower limit on climate sensitivity but probably not a practically useful limit.

Comprehensive study of the relation between solar variability and climate sensitivity would need to account more realistically for the climate forcing change over the solar cycle. One reason that the actual climate forcing is different than in the above idealized experiment is that solar cycle irradiance variations are not spectrally uniform. The range of total (spectrally integrated) solar irradiance is about 0.08% for the most recent complete solar cycle, based on smoothed data of the Active Cavity Radiometer Irradiance Monitor (ACRIM) instruments [*Willson and Hudson*, 1991; *Lean*, 1991; *Willson*, 1994]. However, the range of variability varies strongly with wavelength; J. Lean (private communication, 1995) has provided data indicating that the smoothed range of variability is about 1%, 0.3%, and 0.07% for the spectral intervals less than 0.295 μm, between 0.295 and 0.31 μm, and greater than 0.31 μm, respectively. For a typical zenith angle, solar radiation in these three intervals is absorbed above layer 9 (i.e., above the 10 mbar level), within layer 9 (between 10 and 70 mbar), and beneath layer 9. As these three spectral intervals contain about 0.95%, 0.65%, and 98.4% of the solar irradiance, the proportions of the solar variability associated with the three intervals are about 12%, 2%, and 86%, with the intervals in order of increasing wavelength. Because radiation in the first two intervals is absorbed well above the tropopause while that in the third interval is absorbed mainly at the surface and in the troposphere, the direct climate forcing associated with the solar cycle is approximately 233 W/m^2 × 0.08% × 86% ≈ 0.16 W/m^2.

In addition to this direct solar irradiance forcing, there may be other real-world climate forcings associated with the solar cycle. One of these which can be investigated quantitatively is change of ozone amount. The range of solar cycle variation of ozone amount is about 5 DU (Dobson unit = 2.69×10^{16} molecules cm^{-2}) of ozone in global mean (S. M. Hollandsworth, private communication, 1995), most of the change occurring in our model layers 8 and 9 (between 10 and 150 mbar). In the following section we show how the ozone climate forcing varies with the altitude, latitude and season of the ozone change. For the solar cycle ozone variations of Hollandsworth, these calculations yield a range for the solar cycle ozone forcing of

only about $F_a = 0.05$ W/m^2, which is in phase with the forcing due to the solar irradiance change. Thus the solar cycle ozone forcing is about a factor 3 smaller than the direct solar cycle irradiance forcing.

There may be larger ozone changes associated with solar variability on longer timescales. *Lean et al.* [1995] estimate that ozone may have been reduced 4% (about 12 DU) during the Maunder Minimum, but even this larger ozone reduction yields a forcing only about $F_a = 0.1$ W/m^2 and an equilibrium surface temperature change about 0.1°C. These results suggest that ozone change resulting from solar variability probably is not a substantial contributor to surface climate variability and that the solar-related ozone climate forcing is several times smaller than the direct effect of changing solar irradiance.

The net solar cycle forcing that we have estimated, due to solar irradiance plus ozone changes, is about 0.2 W/m^2. The forcing would be somewhat larger if the solar irradiance measured by Nimbus 7 during its first year of operation is taken literally [*Hickey et al.*, 1988]; these latter data suggest a solar cycle total irradiance variability close to 0.1%, compared to the 0.08% based on ACRIM data alone.

4. Ozone Experiments

The ozone distribution in the control runs for our equilibrium change experiments is shown in Figure 5. Figures 5a and 5b show the ozone amount as a function of height, latitude, and season, while Figures 5c and 5d show the ozone distribution among the 12 layers in our GCM. The global-mean annual-mean ozone amount is 0.306 cm atm or 306 Dobson units (DU). The ozone distribution [*McPeters*, 1993] is representative of measurements for the 1979-1980 period.

4.1. Four Extreme Ozone Perturbations

We first consider four extreme ozone perturbations, using the standard version of the Wonderland model (i.e., calculated clouds or "all feedbacks") to obtain the equilibrium climate response, analogous to the CO_2 and S_0 experiments. Results are shown in Plate 5.

In the first experiment the ozone above the 10 mbar level, 19% of total ozone (Figure 5), is removed. The principal effect is to shift solar ultraviolet heating into the lower atmosphere. The ozone loss also reduces greenhouse warming, but the effect in the troposphere is minor because of its weak coupling to the temperature of the middle and upper stratosphere. Thus the result is a large tropospheric warming (1-3°C) and a very large stratospheric cooling (up to -80°C).

In the second experiment tropospheric ozone is increased, specifically ozone below the 400 mbar level is doubled, yielding a 5.5% increase of total ozone. The principal effect is a greenhouse warming of the troposphere by about 0.5°C. The stratosphere cools, a few tenths of a degree, as the radiation from the troposphere to the stratosphere in the ozone infrared band arises from a higher colder level due to the increased opacity.

In the third experiment ozone in the tropopause region is removed, specifically, all ozone is removed from model layers 7 and 8, which extend from 255 mbar to 70 mbar and contain 16% of the total ozone. Because of the low temperature at this level, ozone is most effective there as a greenhouse material. Thus this ozone change causes a tropospheric cooling, which reaches -4°C near the tropopause and is about -1°C at the surface. This represents a substantial change of tropospheric lapse rate; only a fraction of the upper tropospheric cooling is transmitted to the surface. This contrasts with the CO_2 and S_0 forcings, for which the responses were reasonably uniform through the troposphere. The stratosphere warms in this experiment, because the intensity of radiation upwelling to the stratosphere is increased in the ozone infrared band.

In the fourth experiment, all ozone is removed from the atmosphere. The stratosphere cools by as much as -80°C, but at the surface the change is a cooling of less than 1°C, the impacts of increased solar heating and decreased greenhouse effect coincidentally canceling to first order. Because this experiment is so extreme, we also consider a case with O_3 reduced by half at all levels (Table 3).

These ozone experiments, including the calculated F_t, F_a and ΔT_s for the fixed clouds version of the model, are summarized in Figure 6 and Table 3. The results illustrate that climate response does not have a fixed proportionality to the forcing. In one case (removal of all ozone) the surface temperature response is not even of the same sign as the instantaneous flux change at the tropopause. The adjusted forcing is a much better indicator of the equilibrium response, although the ratio of response to forcing, R, varies by more than a factor of two and it depends substantially on how the clouds are handled.

Quantitative interpretation of these results requires a systematic study of the dependence of the surface temperature change on the location of the ozone change, which we carry out in section 4.2, but understanding of these results requires in turn that we examine a simpler, more general forcing (section 5) and that we quantify specifically the influence of cloud changes (section 6).

4.2. Ozone Sensitivity Profile

We carry out a set of GCM runs with ozone added to each model layer individually, the control run being run 2 (mixed layer ocean). The mean over the last 50 years of each 100-year run is taken as the new equilibrium. The amount of ozone added to a layer is large (100 DU) because we want the calculated surface temperature change to be large compared to the unforced variability in the model. As a result, it is not obvious that the response for smaller perturbations necessarily would scale linearly in ozone amount. Therefore we reran two cases using a 50 DU ozone change, finding that the response was approximately linear in ozone amount. Figure 7 and Table 3 summarize results for the standard climate model and the fixed cloud version.

Figure 7a shows ΔT_s, the equilibrium surface temperature change, and ΔT_0, the calculated surface air temperature change if no climate feedbacks are allowed to operate, as a function of the altitude at which ozone is changed. The ΔT_0 profile can be compared with that calculated by *Lacis et al.* [1990] with a 1-D radiative-convective model. The present result for ΔT_0 versus height is less sharply peaked, with the maximum sensitivity occurring at a lower altitude (≈ 9 km, model layer 6). This is because in our GCM layers 6-8 are in the stratosphere for much of the world, where the ozone change has less impact on the surface, while in the 1-D model the tropopause is at a sharply defined height (just above 12 km).

The principal new result here is the GCM calculation of ΔT_s. With clouds fixed, the dependence of ΔT_s on the altitude of the ozone change (Figure 7a) is qualitatively similar to that of ΔT_0 (or F_a, since $\Delta T_0 \sim 0.3\, F_a$). However, even in this case, ΔT_s is not simply proportional to F_a, and when clouds are free to change, the relation between ΔT_s and F_a becomes complex, i.e., the

Table 3. Ozone Experiments: Radiative Forcings and Equilibrium Responses

Experiment	F_i, W/m^2	F_a, W/m^2	ΔT_0, °C	ΔT_s,°C		$\Delta T_s/F_a$		R	
				Fixed Clouds	All Feedbacks	Fixed Clouds	All Feedbacks	Fixed Clouds	All Feedbacks
No O_3 above 10 mbar	0.55	1.43	0.43	1.34	1.19	0.94	0.83	1.43	1.00
2×O_3 below 400 mbar	0.39	0.32	0.10	0.21	0.46	0.66	1.44	1.00	1.65
No O_3 near tropopause	-0.74	-1.54	-0.45	-1.16	-1.03	0.75	0.67	1.13	0.71
No O_3 anywhere	3.44	-1.67	-0.48	-2.14	-0.52	1.28	0.31	1.92	0.33
0.5×O_3 everywhere	-0.05	-1.43	-0.42	-1.10	-1.04	0.77	0.73	1.15	0.78
100 DU added to layer									
Layer 12	-0.41	-0.17	-0.05	-0.08	-0.05	0.47	0.29	0.71	0.33
Layer 11	-0.55	-0.13	-0.04	-0.04	-0.13	0.31	1.00	0.47	1.12
Layer 10	-0.69	-0.25	-0.07	-0.16	-0.43	0.64	1.72	0.96	1.93
Layer 9	-0.61	0.61	0.18	0.56	0.38	0.92	0.62	1.39	0.72
Layer 8	-0.47	1.91	0.60	1.74	1.31	0.91	0.69	1.39	0.84
Layer 7	4.66	2.98	0.91	1.83	1.28	0.61	0.43	0.95	0.55
Layer 6	4.15	3.31	1.02	1.75	1.82	0.53	0.55	0.82	0.72
Layer 5	3.13	2.70	0.83	1.60	2.36	0.59	0.87	0.91	1.14
Layer 4	2.00	1.74	0.54	1.25	2.34	0.72	1.34	1.10	1.65
Layer 3	1.15	1.02	0.32	0.87	2.32	0.84	2.27	1.30	2.69
Layer 2	0.62	0.54	0.17	0.43	0.87	0.80	1.61	1.21	1.86
Layer 1	0.23	0.19	0.07	0.19	-0.39	1.00	-2.05	1.51	-2.34
O_3 in layers 7 and 8 removed									
All latitudes and seasons	-0.74	-1.54	-0.45	-1.16	-1.03	0.75	0.67	1.13	0.71
High latitudes	-0.52	-0.85	-0.20	-0.67	-0.58	0.79	0.68	1.18	0.75
High latitudes, warm 6 months	-0.27	-0.49	-0.13	-0.38	-0.39	0.78	0.80	1.17	0.88
15 year(1979-1994) ozone change (all feedback runs are 400 years)*									
TOMS/SAGE estimate	0.09	-0.20	-0.06	-0.18	-0.12	0.90	0.60	1.35	0.67
SBUV/SAGE estimate	-0.10	-0.28	-0.08	-0.23	-0.20	0.82	0.71	1.24	0.80

climate response is far from being proportional to the climate forcing. The dependence of climate sensitivity on the location of the ozone change is illustrated more clearly by the feedback factor, $\Delta T_s/\Delta T_0$. The feedback factor depends strongly on the altitude of the O_3 change (Figure 7b), especially if cloud cover is computed.

The most remarkable result is the paradoxic surface cooling that results from ozone added to the lowest atmospheric layer (Figure 7). This is not a consequence of the large value of the ozone forcing (100 DU), as we verified by using a change half as large. We conclude that negative feedbacks can change the sign of the surface temperature response in a GCM, as will be discussed in section 6. Although this conclusion may be counter-intuitive, such intuition derives from 1-D radiative-convective models which suffer from the constraint of a specified tropospheric lapse rate. Such a constraint applies neither to a GCM nor to the real world.

Another conclusion is that the profile of the sensitivity (of surface temperature) as a function of the height of ozone change is broadened by physical processes represented in a GCM. Thus the climate sensitivity to ozone change in the middle troposphere and in the lower stratosphere is larger than would be inferred from a 1-D or 2-D radiative-convective model. Previously, on the basis of calculations of ΔT_0 versus height [*Lacis et al.*, 1990], it has been realized that ozone change near the tropopause is an important climate forcing, but, as shown by Figure 7a, when climate feedbacks are included, the relative importance of tropospheric ozone change is enhanced, as is the importance of ozone changes just above the tropopause.

An approach to quantitative interpretation of the climate response to ozone change is suggested by Figure 7. First, we should analyze how the climate response depends upon location of the forcing in the absence of cloud changes, and, second, we should isolate and analyze the role of cloud changes. These tasks are carried out in the following two sections.

5. Ghost Forcing Experiments

How does the climate response depend upon the time and place at which a forcing is applied? The forcings considered above all have complex temporal and spatial variations. For example, the change of solar irradiance varies with time of day, season, latitude, and even with longitude because of zonal variations in ground albedo and cloud cover. We would like a simpler test forcing.

We define a "ghost" forcing as an arbitrary heating added to the radiative source term in the energy equation [*Hansen et al.*, 1983, Table 1]. The forcing in effect appears magically from outer space at any chosen atmospheric level, latitude range, season, and time of day. Usually, we choose a ghost forcing with global and annual mean 4 W/m^2, making it comparable to the 2×CO_2 and +2% S_0 experiments.

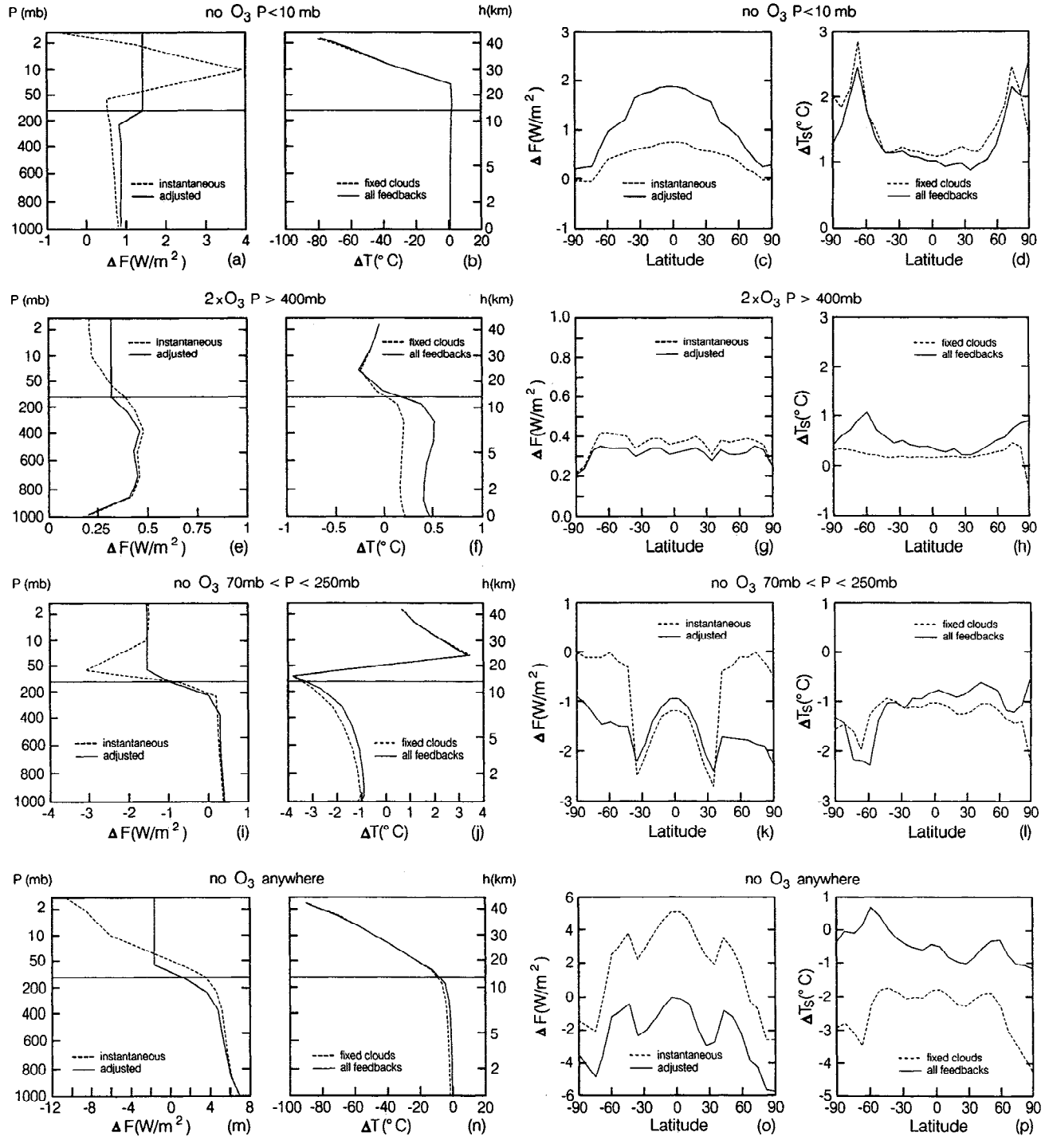

Figure 6. Forcings and responses in four ozone change experiments. The first column is the altitude distribution of the net radiative flux. The second column is the altitude distribution of equilibrium temperature change. The third column is the zonal mean forcing versus latitude. The fourth column is the zonal mean surface temperature response.

5.1. Dependence on Spatial Distribution of Forcing

Height sensitivity. In the first ghost experiments we add 4 W/m² into a model layer uniformly over the globe. The instantaneous forcing F_i, by definition, is 4 W/m² if the ghost forcing is added to a layer lying in the troposphere, zero if the layer is in the stratosphere, and between zero and 4 W/m² if the layer lies partly in the troposphere and partly in the stratosphere (Table 4). The adjusted forcing F_a is similar to F_i for ghost heating added in the troposphere (Table 4), but ghost heating in the stratosphere yields a substantial adjusted forcing, which is a consequence of the increased stratospheric temperature and the resulting infrared flux across the tropopause. Because the infrared opacity in the stratosphere is small at most wavelengths, it is not surprising that the adjusted forcing is about half of the heating added to the stratosphere (Table 4).

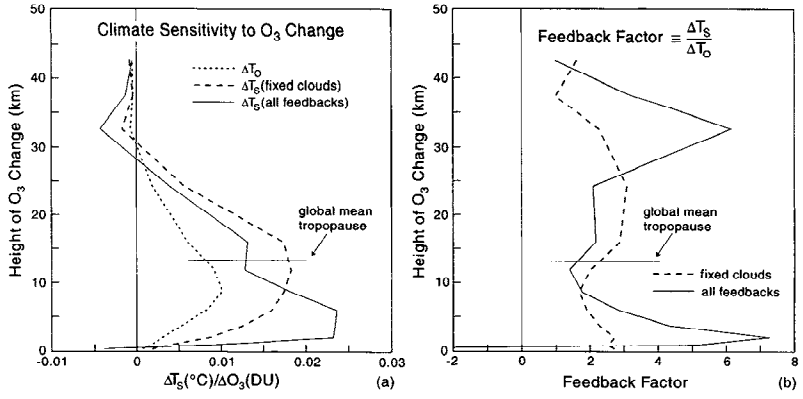

Figure 7. (a) Surface air temperature sensitivity to a globally uniform change of 100 DU atmospheric ozone as a function of the altitude at which the ozone is changed. ΔT_0 is the surface temperature response without any climate feedbacks allowed to operate, i.e., clouds, sea ice, water vapor, and tropospheric lapse rate are fixed (the control run is run 2ciql). (b) Feedback factor, $\Delta T_s/\Delta T_0$, as a function of the altitude at which the ozone is changed.

Table 4. Ghost Forcings and Equilibrium Responses

Ghost forcing	F_i, W/m²	F_a, W/m²	ΔT_0, °C	ΔT_s, °C: Fixed Clouds	ΔT_s, °C: All Feedbacks	$\Delta T_s/F_a$: Fixed Clouds	$\Delta T_s/F_a$: All Feedbacks	R: Fixed Clouds	R: All Feedbacks
4 W/m² into layer 9	0.00	1.83	0.53	1.31	1.12	0.72	0.61	1.09	0.75
4 W/m² into layer 8	1.58	2.86	0.81	2.58	1.94	0.90	0.68	1.39	0.87
4 W/m² into layer 7	2.97	3.58	1.03	2.35	1.71	0.66	0.48	1.01	0.64
4 W/m² into layer 6	3.97	3.96	1.15	2.32	1.88	0.59	0.47	0.91	0.64
4 W/m² into layer 5	4.00	3.98	1.17	2.33	2.12	0.59	0.53	0.91	0.72
4 W/m² into layer 4	4.00	3.98	1.17	2.56	2.38	0.62	0.60	0.95	0.81
4 W/m² into layer 3	4.00	3.98	1.17	2.63	2.26	0.66	0.57	1.02	0.77
4 W/m² into layer 2	4.00	3.97	1.17	2.82	4.20	0.71	1.06	1.10	1.43
4 W/m² into layer 1	4.00	3.98	1.17	2.89	4.88	0.73	1.23	1.13	1.66
4 W/m² into surface	4.00	3.91	1.15	2.83	3.47	0.72	0.89	1.12	1.20
4 W/m² into layers 1-7	3.78	3.89	1.14	2.54	2.50	0.65	0.64	1.01	0.87
8 W/m² at latitudes poleward of 30°									
Into layer 7	1.04	3.04	0.93	2.06	1.66	0.68	0.55	1.04	0.71
Into layer 4	4.00	3.82	1.20	2.53	2.97	0.66	0.78	1.03	1.05
Into layer 1	4.00	3.83	1.21	3.01	6.14	0.79	1.60	1.22	2.16
Into surface	4.00	3.91	1.18	3.02	4.39	0.77	1.12	1.20	1.51
8 W/m² at latitudes equatorward of 30°									
Into layer 7	4.00	4.12	1.11	2.68	1.58	0.65	0.38	1.01	0.52
Into layer 4	4.00	4.14	1.12	2.35	1.68	0.57	0.46	0.88	0.56
Into layer 1	4.00	4.13	1.12	2.59	3.16	0.63	0.77	0.97	1.05
Into surface	4.00	3.90	1.10	2.57	2.37	0.66	0.61	1.02	0.82
Forcings into surface									
8 W/m² NH	4.00	3.87	1.13	2.83	2.43	0.73	0.63	1.13	0.85
8 W/m² SH	4.00	3.94	1.15	2.63	3.15	0.67	0.80	1.03	1.08
16 W/m² 30°N-90°N	4.00	3.85	1.15	2.88	2.51	0.75	0.65	1.16	0.88
16 W/m² 30°S-90°S	4.00	3.96	1.17	2.68	3.82	0.68	0.96	1.05	1.31
4 W/m² lat>30°,-4 W/m² lat<30°	0.00	0.00	-0.08	0.53	1.33	∞	∞	∞	∞
4 W/m² lat<30°,-4 W/m² lat>30°	0.00	0.00	-0.08	-0.68	-2.87	∞	∞	∞	∞
16 W/m² spring	4.00	3.90	1.06	2.86	3.56	0.73	0.91	1.14	1.23
16 W/m² summer	4.00	3.90	1.41	2.72	3.34	0.70	0.86	1.08	1.16
16 W/m² fall	4.00	3.90	1.20	2.83	3.50	0.73	0.90	1.12	1.21
16 W/m² winter	4.00	3.91	0.89	2.91	3.61	0.74	0.92	1.15	1.25
Forcings into layer 1									
8 W/m² day	4.00	3.98	1.20	2.85	5.12	0.72	1.29	1.11	1.75
8 W/m² night	4.00	3.98	1.13	2.91	4.70	0.73	1.18	1.13	1.60

NH, northern hemisphere; SH, southern hemisphere; lat, latitude

The surface temperature change as a function of the altitude of the 4 W/m^2 ghost forcing is shown in Figure 8. The profile of ΔT_0, the temperature change in the absence of feedbacks, is simply a reflection of F_a, to which ΔT_0 is approximately proportional. Our main result is ΔT_s, the GCM calculated surface temperature change when feedbacks are allowed to operate. We show both ΔT_s itself and the feedback factor, $\Delta T_s/\Delta T_0$, and we include results for the standard model and the model with fixed clouds.

We note that the feedback factor for the ghost forcing varies with the altitude of the forcing by about a factor of two. We also note that a substantial surface temperature response is obtained even when the forcing is located entirely within the stratosphere. Analysis of these results requires that we first quantify the effect of cloud changes (section 6). However, the results can be understood qualitatively as follows.

Consider ΔT_s in the case of fixed clouds. As the forcing is added to successively higher layers, there are two principal competing effects. First, as the heating moves higher, a larger fraction of the energy is radiated directly to space without warming the surface, causing ΔT_s to tend to decline as the altitude of the forcing increases. However, second, warming of a given level allows more water vapor to exist there, and at the higher levels water vapor is a particularly effective greenhouse gas. The net result is that ΔT_s tends to decline with the altitude of the forcing, but it has a relative maximum near the tropopause.

When clouds are free to change, the surface temperature change depends even more on the altitude of the forcing (Figure 8). The principal mechanism is that heating of a given layer tends to decrease large-scale cloud cover within that layer. The dominant effect of decreased low level clouds is a reduced planetary albedo, thus a warming, while the dominant effect of decreased high clouds is a reduced greenhouse effect, thus a cooling. However, the cloud cover, the cloud cover changes, and the surface temperature sensitivity to changes may depend on characteristics of the forcing other than altitude, e.g., latitude, so quantitative evaluation requires detailed examination of the cloud changes (section 6).

We conclude that the responsivity R to a globally uniform ghost forcing varies by about a factor of 2 with the altitude of the forcing (Table 4). Also, if the forcing is distributed uniformly through the troposphere, the ghost forcing is about as effective as a solar irradiance forcing of the same magnitude (Table 4).

Latitude sensitivity. A limited examination of the climate sensitivity to the latitude of the forcing is included in Table 4. Specifically, we compared cases in which ghost forcing was added in the northern hemisphere, the southern hemisphere, latitudes equatorward of 30°, and latitudes poleward of 30°. In each case, a heating of 8 W/m^2 was added at the surface, yielding a global mean instantaneous forcing $F_i = 4$ W/m^2.

The difference of climate sensitivity between hemispheres in our model is moderate, the northern hemisphere being more sensitive with clouds fixed and the southern hemisphere being more sensitive with calculated clouds. The latter result occurs because of the positive interaction between calculated clouds and sea ice cover in this GCM, which is most significant in the southern hemisphere. In addition to the uncertainty in the modeling of sea ice/cloud interactions, it should be noted that the present equilibrium mixed layer ocean calculations are most relevant to the century timescale. On shorter timescales the thermal inertia of the ocean probably reduces the transient response more in the southern hemisphere than in the northern hemisphere. On paleoclimate timescales the crucial ice sheet feedback process is expected to be larger in the northern hemisphere, which also increases the expected response relative to that in the southern hemisphere.

A forcing at high latitudes yields a larger response than a forcing at low latitudes. This is expected because of the sea ice feedback at high latitudes and the more stable lapse rate at high latitudes, the latter tending to confine the thermal response to low levels. The largest latitudinal variations occur with calculated clouds. These results are examined in section 6.

5.2. Dependence on Temporal Variation of Forcing

Seasonal sensitivity. Seasonally dependent forcing presents a curious case, revealing a foible of ΔT_0. In four experiments (Table 4) we applied a 16 W/m^2 forcing at the surface each season in the appropriate hemisphere, so that the global-mean annual-mean forcing was 4 W/m^2. The equilibrium response of ΔT_s is rather insensitive to the season, being largest in winter and smallest in summer. This is not surprising, given the larger sensitivity of a colder climate and its more stable lapse rates.

The curious aspect is that ΔT_0 has a strong seasonal dependence and is not proportional to F_a. Results of the ΔT_0 calculation are shown in Figure 9 for the extreme cases of summer and winter forcings. These can be understood from the

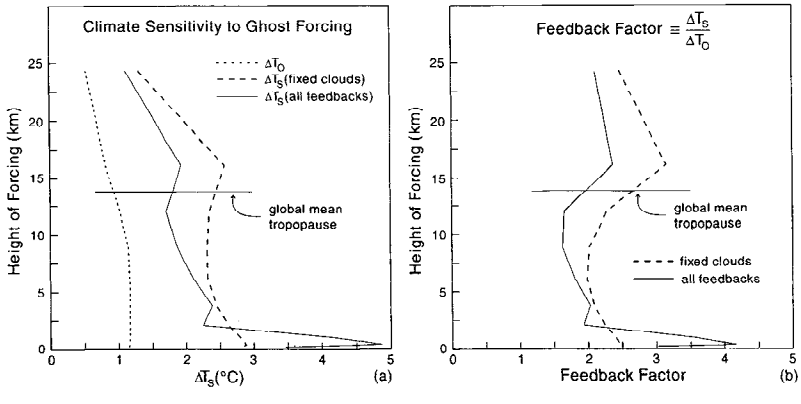

Figure 8. (a) Surface air temperature sensitivity to a globally uniform ghost forcing of 4 W/m^2 as a function of the altitude of the forcing. ΔT_0 is the surface temperature response without any climate feedbacks allowed to operate. (b) Feedback factor, $\Delta T_s/\Delta T_0$, as a function of the altitude at which the ghost forcing is inserted.

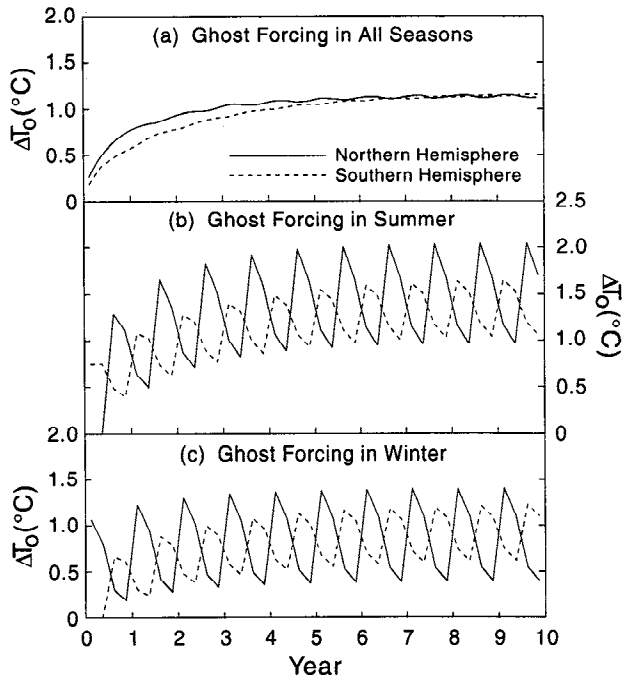

Figure 9. Calculated ΔT_0 for ghost forcings added to the planetary surface (a) 4 W/m² uniformly over the year, (b) 16 W/m² during the summer of each hemisphere (June-July-August (JJA) in northern hemisphere (NH), December-January-February (DJF) in southern hemisphere (SH)), (c) 16 W/m² during the winter of each hemisphere. ΔT_0 is the equilibrium result, which is achieved by year 10.

response time of the mixed layer ocean (several years, given the absence of feedbacks), the radiative relaxation time of the atmosphere (several months), and the fact that the summer troposphere contains more water vapor than the winter troposphere. The greater water vapor in the summer, with its more effective greenhouse trapping, causes the increase of T_0 to be larger in the three months of summer heating. The magnitude of the thermal relaxation in the 9 months following the heating is not sensitive to the season when the heating occurred, so the annual mean of ΔT_0 is higher in the case of summer forcing. In the GCM calculation of ΔT_s, the water vapor, lapse rate, sea ice, atmospheric dynamics, and other feedbacks operate, spreading the impacts of forcings spatially and temporally. It turns out that the equilibrium ΔT_s responds most to the winter forcing, despite the smaller value of ΔT_0, for qualitative reasons mentioned above. Neither F_a nor ΔT_0 is a useful predictor of seasonal climate sensitivity, but F_a, being insensitive to seasonal change, is less deceptive than ΔT_0.

Seasonally dependent forcing is more than a curiosity. Although there is little dependence of the climate response on seasonality of ghost forcings at the surface, other cases are more sensitive. The modeled climate response to ozone depletion exhibits some dependence on the seasons of depletion (Table 3). Even more dramatic dependence on the season of forcing occurs in paleoclimate simulations (not illustrated here). (We carried out a large number of simulations with different earth orbital (Milankovitch) parameters, with the intention of including them as a final section in this paper. The calculations are particularly relevant to the thesis of this paper, because, about as often as not the calculated global mean ΔT_s has the opposite sign of F_a. However, the number of calculations and complexity of this case is so great that it seems better pursued as a separate study.)

Diurnal sensitivity. The model response is not sensitive to the diurnal character of the forcing, judging from the test case in Table 4. In this case a forcing of 8 W/m² was added to layer 1 either in the day or at night, with little difference in the response compared to a uniform 4 W/m². Presumably, this is a consequence of the radiative relaxation time being significantly longer than a day.

6. Cloud Forcing Experiments

We want to understand how the climate responds to a specified change of cloud cover or cloud properties for two reasons. First, imposed cloud changes, for example, those caused by anthropogenic aerosols, are a climate forcing that should be compared to other forcings. Second, cloud changes that occur in response to climate change are a key feedback that we need to analyze.

6.1. GCM Response to Specified Cloud Cover Changes

The spatial distribution of clouds in the GCM control run is illustrated in Plate 6. We determine the climate model's sensitivity to cloud cover change by arbitrarily increasing the large-scale clouds in a given model layer. In each case we increase the cloud cover by 5% of the global area, by adding clouds in regions that are cloud-free in all layers of the control run. Thus, for example, the cloud cover in layer 1 is increased from the 32.5% in the control run to 37.5%. The optical depth of the added clouds is the same as that of the other large-scale clouds in that layer, as defined in Table 5. The control run has clouds only in layers 1-7, but for didactic purposes we included cloud forcing in layers 8 and 9. The geographical and height distributions of clouds in the control run are shown in Plate 6.

Figure 10 and Table 5 show that, on global average, the albedo effect of clouds below 7-8 km altitude dominates over their greenhouse effect and thus they cause a global cooling, while the opposite is true for higher clouds (if they are not too optically thick), consistent with earlier results [*Manabe*, 1975; *Stephens and Webster*, 1981].

6.2. Analysis of Cloud Feedback Effect

We use the GCM's sensitivity to specified cloud changes to estimate the contribution of cloud feedbacks to climate sensitivity in the ghost and ozone experiments that were carried out with the standard (all feedback) version of the GCM. Many feedbacks contribute to the difference in the responses of the "fixed clouds" and "all feedbacks" models, including cloud changes as a function of height, latitude, season and time of day, as well as water vapor, sea ice, and dynamical changes. However, we anticipate that the cloud changes themselves will be the dominant mechanism, and among those, the above experiments suggest that the main effect may be cloud change as a function of height.

We first illustrate the annual-mean global-mean temperature and cloud cover changes that occur in the ghost and ozone experiments. We then estimate quantitatively the contributions of the principal cloud changes to the temperature change.

Cloud feedbacks are simplest for the ghost forcing. Figure 11 shows the temperature changes and cloud changes that occur in the GCM when a globally uniform ghost forcing is added at one of four different levels: the surface, layer 1, layer 4, and layer 7.

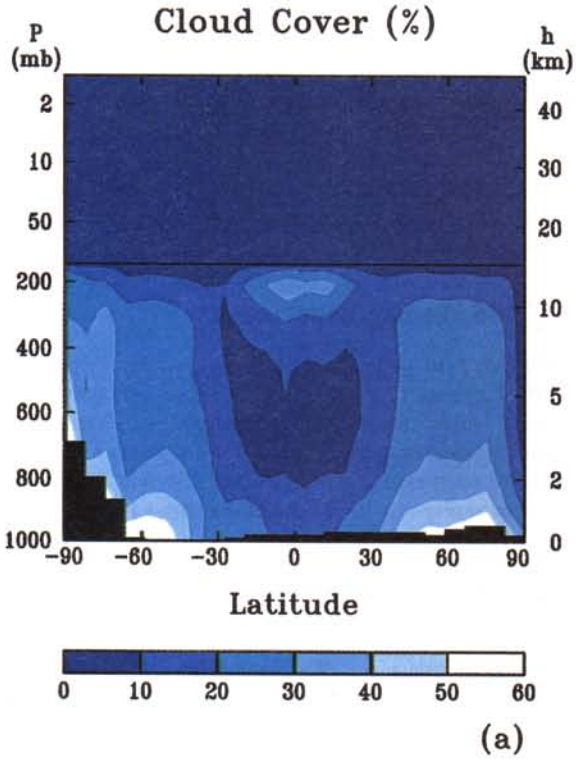

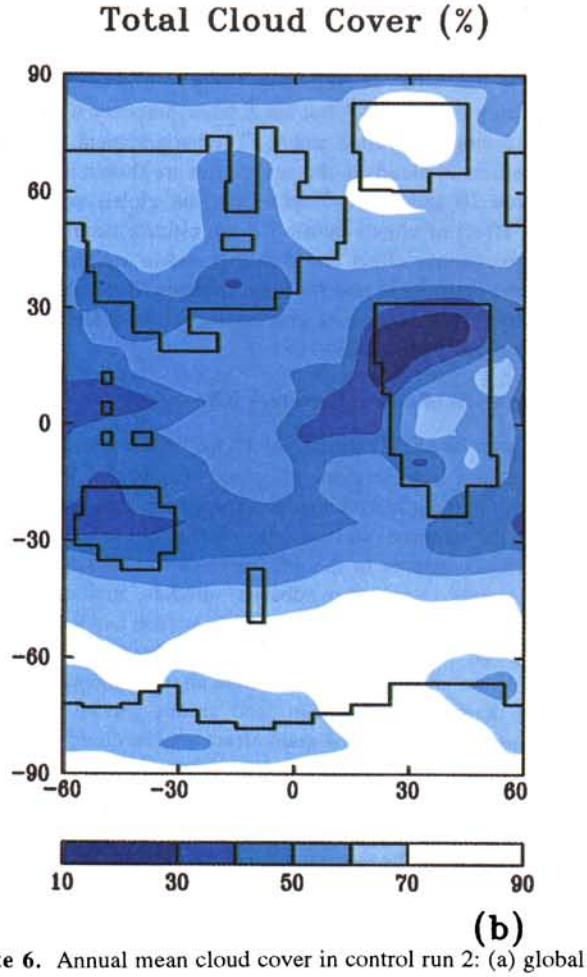

Plate 6. Annual mean cloud cover in control run 2: (a) global distribution of total cloud cover, and (b) latitude-height distribution of clouds.

Calculated clouds are a positive feedback for a ghost forcing added in the lower troposphere, neutral for a forcing in the mid troposphere, and a negative feedback for an upper tropospheric ghost forcing.

The principal effect of the ghost heating on cloud cover is a reduction of large-scale clouds within the layer that is heated, as illustrated in Figure 11e. This mechanism qualitatively explains the dependence of the cloud feedback on the altitude of the ghost forcing, as reduction of low level clouds causes warming, while reduction of high clouds causes cooling. A second effect of the ghost heating is to increase the local static stability, thus decreasing convection from below; in the lower part of the troposphere this reduced convection increases the cloud cover in the layer below. This second effect reduces the positive cloud feedback in the low troposphere, and it eliminates the positive feedback in the middle troposphere. When the ghost heating is added to layer 1, however, there is no lower layer with a negative feedback, so this case yields the strongest positive feedback. Finally, we note that surface warming causes an increase of high level clouds, which is one reason that the GISS GCM has a relatively high climate sensitivity [*Hansen et al.*, 1983].

The cloud feedback for ozone change (Figure 12) has some characteristics in common with the ghost forcing (Figure 11), but ozone change, because ozone effectively emits thermal radiation and absorbs solar radiation, alters the amount of heat added to a layer in a more complicated way. Consider first the case when ozone is added to layer 1. The added ozone allows layer 1 to cool to space more effectively (via the 9.6 μm ozone band, in the middle of the Earth's infrared "window"), thus lowering the temperature of layer 1 and increasing the cloud cover there. Cooling from the added clouds exceeds warming from the added ozone. When ozone is added to layer 3, it cools that layer and thus slightly increases cloud cover there; but the decreased vertical stability decreases cloud cover in layers 1 and 2 (Figure 12e), and thus the net effect of the ozone and cloud changes is a strong warming (Figure 12b). When ozone is added to layer 7, which is near a minimum in the vertical profile of temperature, it warms that layer and thus decreases the large-scale cloud cover there.

Now let us examine how well the cloud cover changes can "explain" the climate model sensitivity when all feedbacks are allowed to operate. First, consider the "paradoxical" case in which ozone added to layer 1 causes a planetary cooling. Table 6 gives the annual-mean global-mean cloud cover change (δC) for each atmospheric level. Table 6 also gives an estimate of the contribution to the surface temperature change from the cloud change in each layer (δT_s) based on the ΔT_s/cloud cover relation from Table 5. The sum of the δT_s for all layers is -0.59°C, essentially the same as the difference in ΔT_s between the fixed cloud and calculated cloud GCM experiments (-0.58°C). This nearly perfect agreement is accidental, but similar checks for ozone changes in other layers (Table 6) confirm that the mean cloud change with altitude accounts for most of the difference between the climate sensitivities with fixed clouds and calculated clouds, in the case of ozone forcing.

This simple calculation, accounting only for the altitude dependence of the cloud change, does not explain the effect of calculated clouds on climate sensitivity so accurately in all cases. The latitude dependence of the cloud change also affects the simulated surface temperature change; the principal latitudinal variation is between low latitudes and high latitudes, with a smaller variation between hemispheres (Table 7). Furthermore, the sensitivities to cloud changes (Table 5) were obtained by

Table 5. Global Mean Cloud Cover and Optical Depth in Control Run

Layer	Pressure mbar	Cloud Cover, %	Optical Depth	F_i, W/m²	F_a, W/m²	ΔT_0, °C	ΔT_s, °C	$\Delta T_s/F_a$	R
			Cloud Cover in Layer n Increased 5%						
9	10-70	0.0	1/3	0.72	0.90	0.26	0.70	0.78	1.18
8	70-150	0.0	1/3	1.04	1.04	0.29	0.98	0.94	1.43
7	150-255	20.3	1.3	1.16	1.16	0.33	0.69	0.59	0.91
6	255-390	18.4	3.0	0.76	0.74	0.21	0.45	0.61	0.92
5	390-550	15.3	4.9	-0.92	-0.91	-0.27	-0.45	0.49	0.74
4	550-720	16.2	7.1	-3.02	-3.04	-0.91	-1.62	0.53	0.79
3	720-854	19.6	9.1	-4.54	-4.48	-1.30	-2.70	0.60	0.88
2	854-934	28.2	10.6	-5.18	-5.22	-1.52	-3.37	0.65	0.94
1	934-984	32.5	11.4	-5.60	-5.60	-1.66	-3.84	0.69	1.00
			Optical Thickness in a Layer Doubled						
7	150-255	20.3	2/3	2.72	2.69	0.78	1.55	0.58	0.89
2	854-934	28.2	21.2	-4.00	-3.97	-1.20	-2.94	0.74	1.09
1	934-984	32.5	22.8	-3.93	-3.90	-1.20	-3.12	0.79	1.18

Radiative forcings and equilibrium responses are for nine experiments in which cloud cover of a layer is increased 5% of global area, and three experiments in which optical depth in a layer is doubled.

adding clouds in regions that were cloud-free in all layers, which tends to overestimate the effect of the cloud change for other situations. A more precise accounting requires consideration of cloud overlap effects.

6.3. Other Cloud Forcings

Cloud forcings, in addition to change of cloud cover, include change of cloud height, cloud optical thickness, cloud liquid water content, and cloud particle size, but the effect of changing cloud height is implicitly included in our tabulated results for change of cloud cover (Table 5). For any cloud height change of interest it is only necessary to determine the corresponding change of cloud cover in our fixed atmospheric levels and sum over the nine levels.

Similarly, although we have not explicitly examined the effects of changing either cloud liquid water content or cloud particle size, the climate sensitivity to changes of these parameters can be inferred from the sensitivity to changes of cloud optical thickness to a reasonable approximation, assuming that the cloud particles are sufficiently large, say greater than 5 μm in effective radius. Therefore we include in Table 5 the sensitivity of climate forcing and climate response to change of optical thickness for low clouds and high clouds.

As expected, an increased opacity of optically thin high clouds causes warming while increased opacity of low clouds causes cooling. The sensitivities indicated are only valid for small perturbations about today's climatology. Indeed, as is well known, the effect of clouds on infrared radiation saturates at a smaller optical depth than does the cloud albedo, so if the optical depth of high clouds becomes large enough the clouds cause a cooling. *Lacis et al.* [1979] find that the maximum greenhouse effect for high level clouds occurs at optical depth about 2, and the effect shifts to cooling only for optical depths greater than about 10, the optical depth of this switchover depending on cloudtop temperature.

7. Chlorofluorocarbon (CFC) Experiments

The increase of radiative forcing due to chlorofluorocarbons, which are entirely of anthropogenic origin, has exceeded the radiative forcing of all other greenhouse gases except CO_2 for the past three decades [*Hansen et al.*, 1989]. Thus it is important that the CFC forcing be accurately determined. Also it is of special interest to examine the net forcing due to CFC plus ozone changes, as observed ozone depletion is presumed to be caused primarily by CFCs. We calculate here the radiative forcings by CFC-11 (CCl_3F) and CFC-12 (CCl_2F_2), which cause most of the current CFC radiative forcing [*Hansen et al.*, 1989; *IPCC*, 1992]. Other CFCs will become relatively more important in the future as the abundances of CFC-11 and CFC-12 are expected to decline, and all of the CFCs must be included in projections of future changes of radiative forcing.

7.1. CFC Vertical Profile

CFCs, because of their long lifetimes, are reasonably well-mixed in the troposphere, but because CFCs decompose in the stratosphere, we must consider how their abundance decreases with altitude. Assumptions used in the literature range from (1) homogeneous mixing throughout the atmosphere to (2) homogeneous mixing up to 12 km (H_0) and then exponential decrease toward higher altitudes with 3 km scale height (H). Atmospheric data [*Kawa et al.*, 1993] suggest that an intermediate assumption, (3) uniform mixing to $H_0 = 16$ km and then exponential decrease with $H = 10$ km scale height, is a more realistic approximation. This is confirmed by recent satellite measurements of CFC-12 profiles as a function of latitude [*Nightingale et al.*, 1996].

We compare the forcings and climate model responses for all three of these height profiles in Table 8. The integrated CFC amount for the most realistic height profile ($H_0 = 16$ km, $H = 10$ km) falls about midway between the amounts for the two extreme cases, but F_a, ΔT_0 and ΔT_s for the most realistic case are closer to the case with homogeneous mixing because CFCs at the highest altitudes become a less effective climate forcing, as we documented for the ghost forcing (Table 4 and Figure 8). The most commonly used CFC distribution, uniform mixing, overestimates the forcing by about 8% (under the assumption

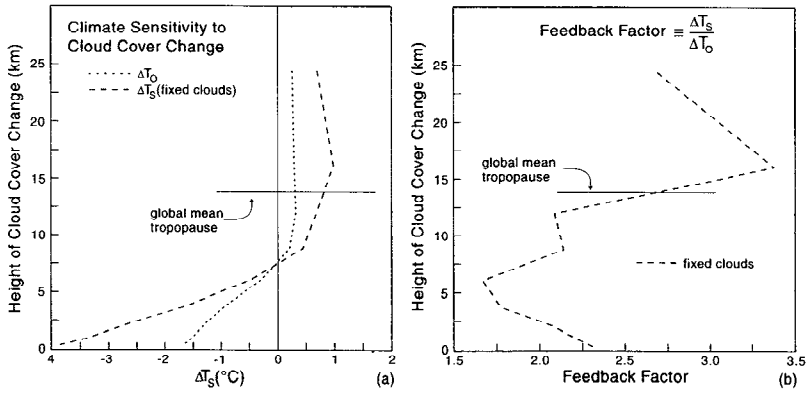

Figure 10. (a) Surface air temperature sensitivity to a globally uniform change of +5% cloud cover as a function of the altitude of the cloud change. ΔT_0 is the surface temperature response without any climate feedbacks allowed to operate. (b) Feedback factor, $\Delta T_s/\Delta T_0$, as a function of the altitude at which the cloud cover is changed.

that H_0 = 16 km, H = 10 km adequately approximates the effect of actual latitude dependent profiles). The CFC profile with H_0 = 12 km and H = 3 km, although perhaps realistic for middle latitudes, underestimates the global F_a by about 18%.

Thus variations of the assumed CFC vertical profiles are a significant cause of differences among the climate forcings calculated by different investigators. The dependence of the forcing on the CFC profile provided in Table 8 can be used to scale the results of any model for one assumed profile to another profile, provided that the assumed profile has been specified. For example, *Pinnock et al.* [1995] point out that their forcing for CFC-11 is 30% greater than that assumed by *IPCC* [1992], the latter being based on 1-D radiative-convective model results given in Appendix B of *Hansen et al.* [1988]. However, Pinnock et al. employed uniform mixing (K. Shine, private communication, 1996) while the equation of Hansen et al. was based on 1-D model calculations for a midlatitude atmosphere with CFC-11 having the H_0 = 12 km, H = 3 km vertical distribution Thus the vertical distributions account for a forcing difference of (1.08 - 0.82)/0.82 ≈ 32%, that is, the different vertical distributions appear to be a major cause of the difference in radiative forcings. This case illustrates the importance of both using a realistic distribution and specifying the distribution that is used.

Another source of differences among models is the assumed absorption coefficients. CFC-11 absorption coefficients in previous GISS radiation calculations were based on work by *Nanes et al.* [1980]. However, more recent data of *Li and Varanasi* [1994], as well as the average of all data compiled by N. Christidis and K. Shine (private communication, 1996), suggest a value 10% higher, which we have adopted here. The CFC-12 absorption coefficient used here is that of *Morcillo et al.* [1966].

Still other sources of differences among the models arise from model dimensionality (low dimension models requiring approximations for integrating over space, season, and cloud effects) and other approximations in the radiative calculations. Our present 3-D calculations explicitly and accurately average over space and time, including a realistic amount and distribution of clouds. The radiative transfer scheme used here is that of *Lacis and Oinas* [1991], with the thermal spectrum divided into bands of approximately 100 wavenumber width, each spectral band being characterized by a full range of absorption coefficient values which are then regrouped into 25 k intervals for efficient

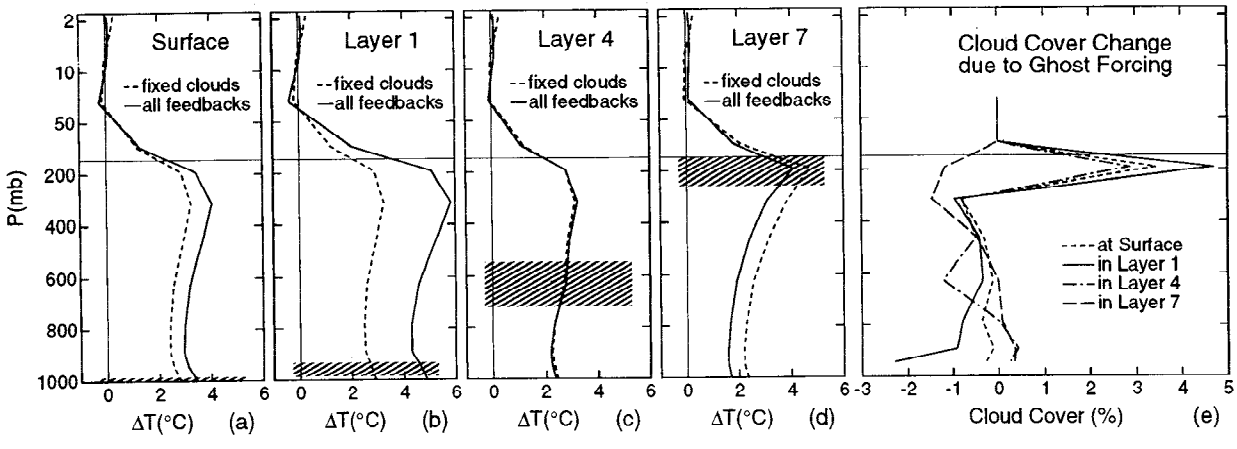

Figure 11. Annual-mean global-mean changes of vertical temperature profile when ghost forcing of 4 W/m^2 is added to (a) the surface, (b) layer 1, (c) layer 4, and (d) layer 7. (e) Cloud cover changes in these four experiments. Shaded areas mark the altitudes of the forcings.

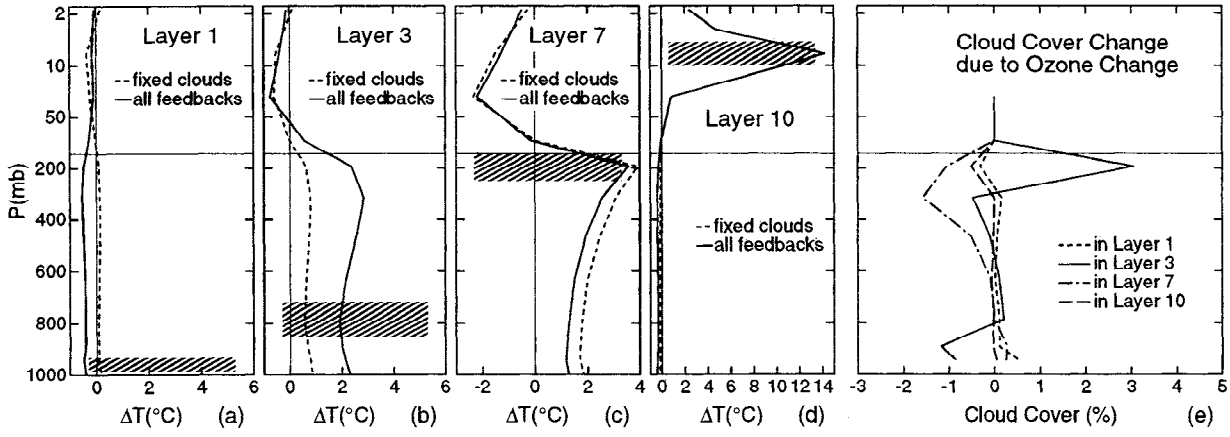

Figure 12. Annual-mean global-mean changes of vertical temperature profile when 100 DU of O_3 is added to (a) layer 1, (b) layer 3, (c) layer 7, and (d) layer 10. (e) Cloud cover changes in these four experiments. Shaded areas mark the altitudes of the forcings.

doubling-adding radiative calculations. For simplicity, CFC absorption in the GISS GCM is applied as a constant across the relevant ($\approx$ 100 wavenumber) spectral interval (weak line approximation); although this approximation makes the nonlinearity of CFC absorption weaker than in the real world, it has negligible impact for realistic CFC amounts.

Our current best estimate for CFC forcings, as specified in Table 8, is 0.063 W/m^2 for 250 ppt of CFC-11 and 0.15 W/m^2 for 500 ppt of CFC-12, the approximate concentrations of recent years; results vary linearly for smaller amounts. By comparison, the parameterizations in Appendix B of *Hansen et al.* [1988] yield values of 0.055 W/m^2 and 0.14 W/m^2, respectively. Thus our present CFC forcings, based on 3-D calculations with H_0 = 16 km, H = 10 km, are only about 5% greater than our earlier results based on 1-D calculations with H_0 = 12 km, H = 3 km when we use the same CFC absorption coefficients as used by *Hansen et al.* [1988]. It follows that for the same CFC vertical distribution, the GCM yields a forcing about 10% smaller than that obtained from the 1-D model. In other words, in comparing our present best estimate for the CFC-11 forcing with the result of *Hansen et al.* [1988], there is a decrease in the calculated forcing arising from use of the GCM to average over the world which partially cancels increases due to the new CFC-11 absorption coefficient and the more realistic vertical distribution of CFCs (H_0 = 16 km, H = 10 km). As the GCM explicitly averages over season, latitude, and cloudy and cloud-free situations, the present results represent our best estimate for the CFC forcings.

Finally, we compare our present CFC forcing with recent results of *Pinnock et al.* [1995]. Their calculated forcing for 250 ppt of CFC-11 is 0.067 W/m^2. *Pinnock et al.* [1995] employ a uniform mixing of CFCs, implying that we must reduce their result by 8% to make it comparable to our computations with H_0 = 16 km, H = 10 km. This makes their result 0.062 W/m^2, almost the same as our result. Such precise agreement is probably accidental; it seems likely that there are compensations among any differences in radiative approximations and integrations over the globe. Despite the close agreement of our results, we estimate that there remains an absolute uncertainty in the CFC-11 forcing of the order of 10%.

7.2. CFCs Versus O_3: An Extreme Experiment

As CFCs are known to cause ozone depletion in the tropopause region, it is of interest to compare CFC and O_3 radiative forcings and climate responses. As a first experiment we use the CFC amount required to yield F_s equal in magnitude to the

Table 6. Estimated Contributions to ΔT_s From Cloud Cover Changes (Approximated as Globally Uniform) in Four Ozone Experiments and Comparison With the Difference Between GCM Calculated ΔT_s in Standard and Fixed Cloud Models

	O_3 in layer 1		O_3 in layer 3		O_3 in layer 7		O_3 in layer 10	
	δC, %	δT_s, °C	δC, %	δT_s, °C	δC, %	δT_s, °C	δC, %	δT_s, °C
Layer 7	-0.32	-0.04	3.05	0.42	-1.06	-0.15	-0.52	-0.07
Layer 6	0.16	0.01	-0.48	-0.04	-1.58	-0.14	0.00	0.00
Layer 5	0.06	-0.01	-0.10	0.01	-0.52	0.05	-0.02	0.00
Layer 4	0.02	-0.01	0.11	-0.04	-0.09	0.03	-0.06	0.02
Layer 3	0.11	-0.06	0.21	-0.11	0.01	-0.01	-0.02	0.01
Layer 2	0.11	-0.07	-1.18	0.80	0.28	-0.19	-0.03	0.02
Layer 1	0.54	-0.41	-0.86	0.66	0.26	-0.20	0.05	-0.04
Sum of δT_s		-0.59		1.69		-0.61		-0.06
ΔT_s		-0.58		1.45		-0.55		-0.17

Table 7. Adjusted Radiative Forcings and Equilibrium Responses for Experiments in Which Cloud Cover in a Given Layer is Increased 5% at Latitudes Poleward of 30° and Equatorward of 30°

Layer		F_a, W/m²		ΔT_s, °C		$\Delta T_s/F_a$		R	
		> 30°	< 30°	> 30°	< 30°	> 30°	< 30°	> 30°	< 30°
7	NH	0.26	0.33	0.16	0.17	0.62	0.52	0.96	0.80
	SH	0.22	0.31	0.10	0.17	0.45	0.55	0.71	0.86
4	NH	-0.54	-0.88	-0.32	-0.47	0.59	0.53	0.92	0.83
	SH	-0.48	-0.95	-0.26	-0.52	0.54	0.55	0.84	0.86
1	NH	-1.12	-1.55	-0.83	-0.96	0.74	0.62	1.16	0.97
	SH	-1.09	-1.59	-0.86	-0.94	0.79	0.59	1.23	0.92

forcing caused by removing all ozone from layers 7 and 8 (70-255 mbar), i.e., F_a = 1.54 W/m². Because the CFC and ozone forcings are of opposite sign, when they are inserted simultaneously into the Wonderland model the climate response should be negligible if different forcings are approximately equivalent.

One reason to employ balanced forcings is that the sensitivity of the climate model, and presumably the real world, is larger for a finite negative forcing than for a positive forcing of equal magnitude (compare S_0 experiments; the main reason for the larger response toward a colder climate is the greater sea ice change). This bias in the response is largely avoided with balanced forcings, a technique which we also used above for ghost forcings and will employ below for aerosols and greenhouse gases.

Plate 7 and Table 8 show that with fixed clouds the net zero forcing yields only a small global mean temperature change (ΔT_s = -0.14°C) if clouds are fixed, but a strong global warming (ΔT_s = 0.81°C) if clouds are calculated. The strongest warming occurs at the locations (high latitudes) which have a strong negative forcing (Plate 7b). Thus this case clearly illustrates the absence of proportionality between radiative forcing and climate response, both globally and regionally.

The reasons for this superficially anomalous response are readily understandable. Plate 7b shows that the null global-mean adjusted forcing is achieved via positive forcing at low latitudes and negative forcing at high latitudes. By itself, this factor would cause the global mean response to be a cooling because, as we have shown, high latitudes are more sensitive to a given radiative forcing than are low latitudes. However, another important factor is the altitude distribution of the levels at which the radiative energy input occurs, which is shown in Figure 13. The negative ozone forcing occurs near the tropopause, while the CFC forcing is weighted more toward the surface, where a forcing is more effective at altering surface temperature, especially at high latitudes, as we have shown in earlier sections. The resulting response to the net CFC and O_3 forcing is consistent with the results for the two individual forcings (sections 4 and 7.1).

7.3. O_3 Forcing: 1979-1994

The above CFC-O_3 comparison illustrates our thesis that equal forcings do not necessarily yield similar climate responses. But a more relevant case is to compare the forcings and responses for measured changes of CFCs and O_3. A difficulty with this case is that the real-world changes of O_3 are not measured precisely.

Table 8. CFC Experiments: Radiative Forcings and Equilibrium Responses

Experiment	F_i, W/m²	F_a, W/m²	ΔT_0, °C	ΔT_s, °C		$\Delta T_s/F_a$		R	
				Fixed Clouds	All Feedbacks	Fixed Clouds	All Feedbacks	Fixed Clouds	All Feedbacks
Tropospheric CFC-11 = CFC-12 = 8.5 ppb[a]									
H_0=12 km, H=3 km	3.45	3.50	1.01	2.59	4.08	0.74	1.17	1.14	1.54
H_0=16 km, H=10 km	4.06	4.29	1.24	3.13	4.62	0.73	1.08	1.13	1.48
H_0= ∞	4.30	4.63	1.34	3.36	4.76	0.73	1.03	1.13	1.44
Tropospheric CFCs with H_0=16 km, H=10 km									
CFC-11=0.25 ppb		0.063							
CFC-12=0.50 ppb		0.150							
CFC-11 = CFC-12 = 2.9 ppb and no O_3 in layers 7 and 8									
	0.25	0.00	0.00	-0.14	0.81	∞	∞	∞	∞

[a] These CFC amounts are less than what would be required to produce the indicated forcings if the radiative transfer in the GCM were carried out with high spectral resolution. For simplicity, the CFC absorption in the GISS GCM is applied as a constant across the relevant spectral band (a "weak line" approximation). Thus the nonlinearity with CFC amount is weaker than in the real world. This approximation has negligible impact for realistic CFC amounts.

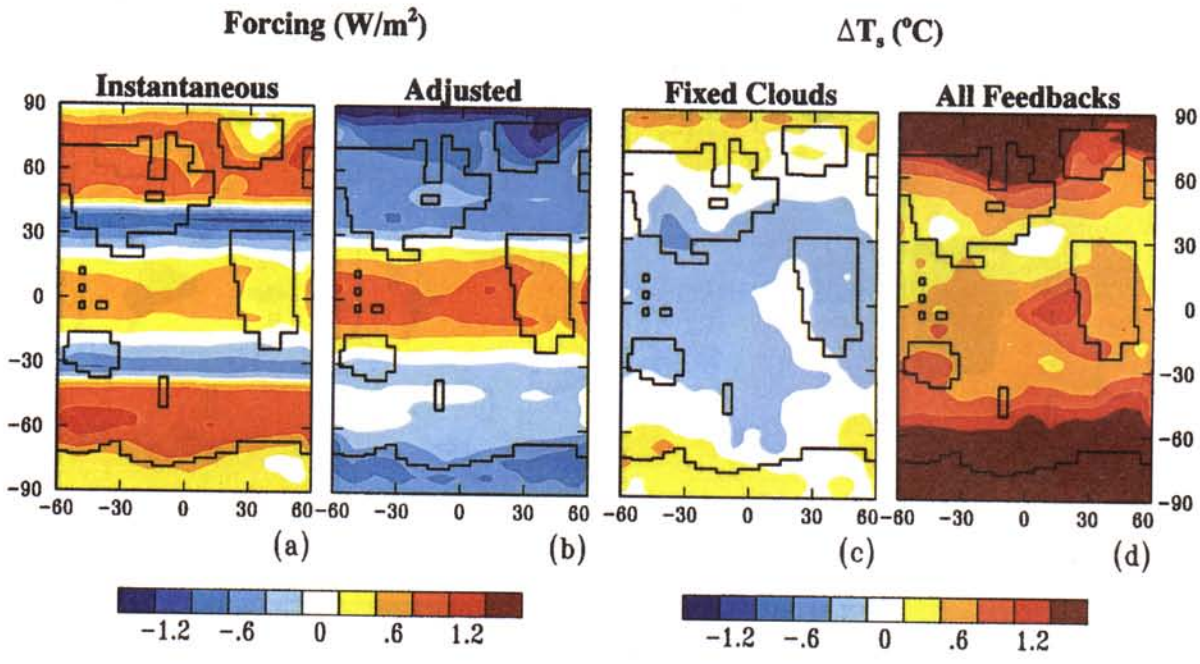

Plate 7. Forcing and response in an experiment with all O_3 removed from layers 7 and 8 (70-255 mbar) and 2.7 ppb of both CFC-11 and CFC-12 added in the troposphere so as to yield zero adjusted forcing (see text): (a) instantaneous forcing, (b) adjusted forcing, (c) equilibrium T_s response for fixed clouds, and (d) equilibrium T_s response for calculated clouds.

As a specific example, consider the two profiles of O_3 change shown in Figure 14a. Profile A, used by *Hansen et al.* [1993a, 1995b], was constructed from Stratospheric Aerosol and Gas Experiment (SAGE) [*McCormick et al.*, 1992] and Total Ozone Mapping Spectrometer (TOMS) [*Stolarski et al.*, 1991] data by using SAGE for the latitude-dependent vertical profile of O_3 change down to 17 km altitude and constraining the ozone amount below 17 km to match the column O_3 change measured by TOMS. Profile B, used by J. Hansen et al. (manuscript in preparation, 1997), was constructed from an updated version of SAGE data (J. Zawodny, private communication, December 1994) and solar backscattered ultraviolet (SBUV) data [*Hollandsworth et al.*, 1995] after using data from several (northern hemisphere) ozonesonde stations [*Logan*, 1994] to specify a tropospheric ozone change profile for latitudes northward of 30°S; SBUV was used to specify the O_3 change profile above the 32 mbar level (~24 km), SAGE was used between 32 and 125 mbar (~24-15 km), with the O_3 change in model layers 1-7 adjusted to yield the SBUV column O_3 change. The profile B changes are specified in greater spatial and temporal detail by Hansen et al. (manuscript in preparation, 1997). Profiles A and B thus are dependent on arbitrary assumptions about tropospheric ozone change, as well as imprecisions in the satellite measurements. Recent reanalyses of the satellite data suggest some changes to the SAGE profiles [*Wang et al.*, 1996; *Cunnold et al.*, 1996] and a somewhat reduced ozone depletion from (version 7) TOMS (R. D. McPeters, private communication, 1996). However, these changes should not qualitatively alter our conclusions here. Indeed, we mention below empirical evidence that the radiative forcing we obtain with profile B is realistic.

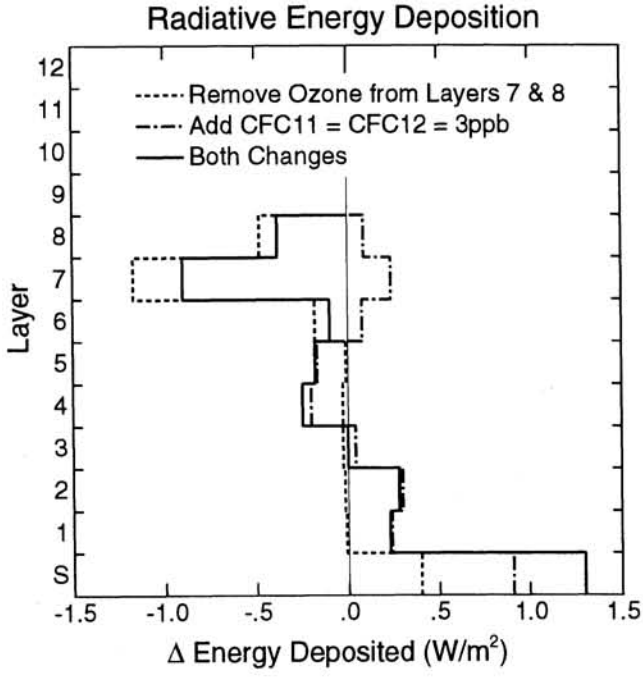

Figure 13. Change of energy deposited in GCM layers and at the surface (S) for the experiment with ozone removed from layers 7 and 8 and CFCs added so as to yield a null adjusted radiative forcing.

Although ozone profiles A and B are superficially similar, the climate forcing is about 40% larger for profile B than for profile A (Table 3), and the calculated equilibrium climate response is similarly larger for profile B (27% for fixed clouds, 67% for calculated clouds). The principal cause of temperature change for both the profile A and profile B experiments is the ozone depletion near the tropopause, especially in model layer 8 (70-150 mbar), but the main cause of the difference between the

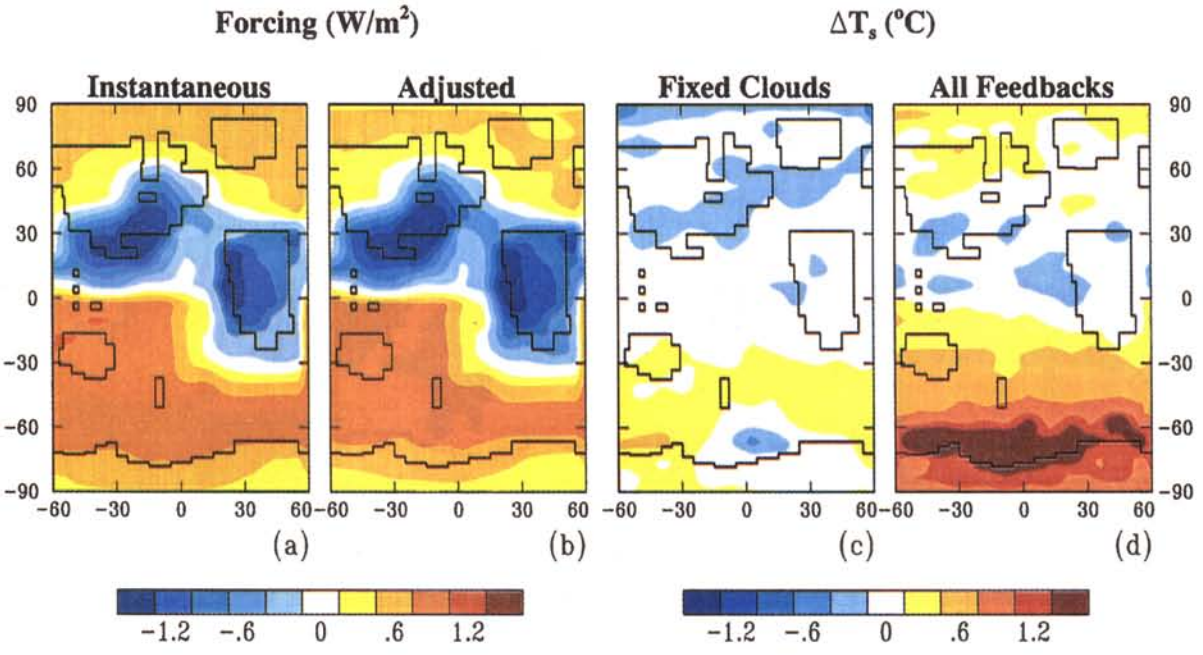

Plate 8. Forcing and response in an experiment with conservatively scattering tropospheric aerosols ($\varpi = 1$) and greenhouse gases, with the amounts chosen to yield zero global-mean adjusted forcing. Aerosol global-mean optical depth is 0.034; the geographical distribution, given in Figure 16 of *Hansen et al.* [1993a], is intended to represent sulfates and biomass burning.

profile A and B results (for both F_a and ΔT_s) is the difference in the tropospheric ozone changes between A and B. This conclusion is obtained by summing the expected contributions (to F_a and ΔT_s) from individual layers, but it is also suggested by comparison of the ΔO_3 and ΔT profiles in Figure 14. Thus reliable assessment of the climate forcing due to ozone change requires improved knowledge of the ozone change at tropospheric levels. This is true for ozone change on the century timescale [*Hauglustaine et al.*, 1994] as well as shorter timescales.

We cannot prove which of profiles A and B is more realistic; indeed, the true profile of ozone change may fall outside the range of these two estimates. The tropospheric ozone changes in profile B are at least based on tropospheric measurements, but the stations are confined to the northern hemisphere [*Logan*, 1994] and do not sample well tropical regions where biomass burning may be causing an increase of tropospheric ozone [*Jiang and Yung*, 1996]. Overall, profile B is based on more observations of profile change, and we believe that it is the more realistic of the two profiles.

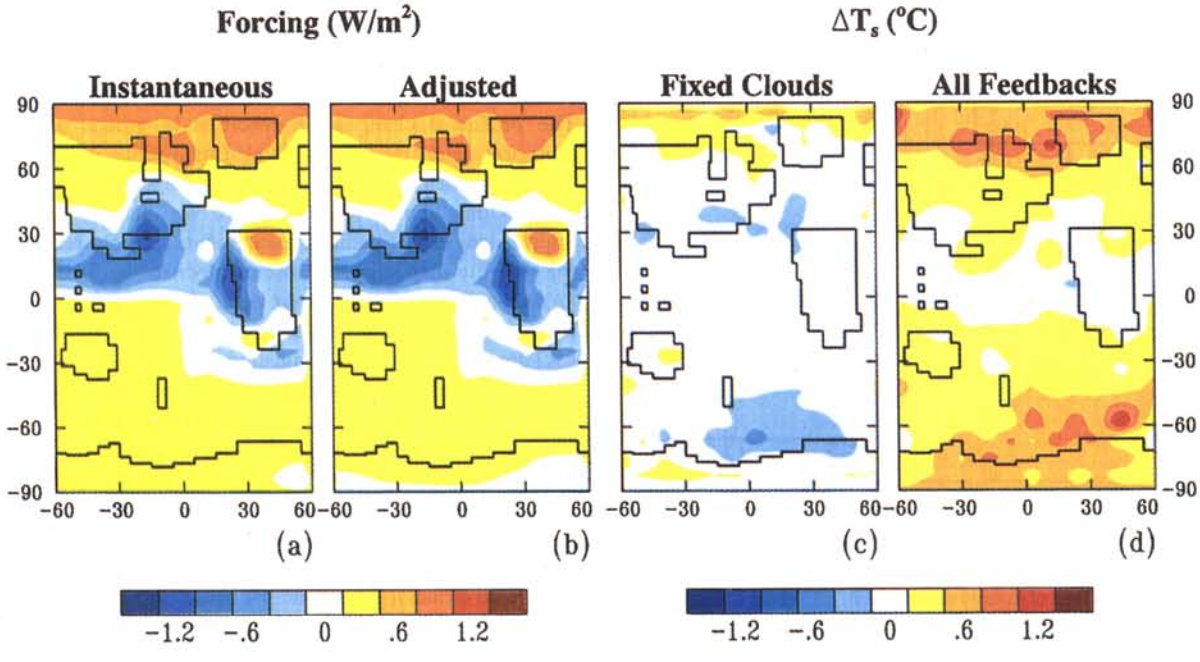

Plate 9. Same as Plate 8 but for absorbing ($\varpi = 0.9$) tropospheric aerosols

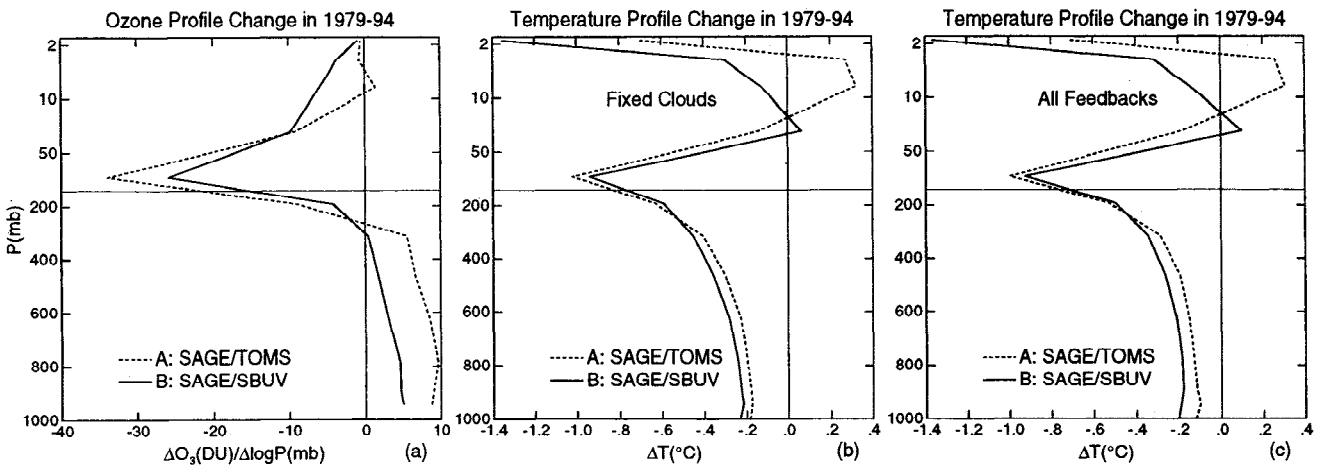

Figure 14. (a) Ozone change profile (global-mean, annual-mean) for the 15-year period 1979-1994 based on two sets of assumptions defined in the text; ozone change is in Dobson units within each of 12 discrete model layers. (b) Temperature change calculated for the assumed ozone change profiles, with fixed clouds. (c) Same as Figure 14b, but with calculated clouds.

The radiative forcings and climate responses calculated with profiles B and A lead us to suggest that the climate effects of ozone change are larger than has generally been believed. For example, *IPCC* [1994, 1995] estimates the forcing due to ozone depletion as -0.1 W/m^2, a factor of 2-3 smaller than our result. The IPCC result is based in part on the forcing calculated by *Ramaswamy et al.* [1992], who obtained F_s = -0.08 W/m^2 for satellite-observed ozone changes in the period 1979-1990 (which scales to -0.11 W/m^2 for 1979-1994), and a similar result of *Schwarzkopf and Ramaswamy* [1993]. Both of these results were obtained with 2-D radiative models. To investigate the reasons for their smaller forcing, we made calculations with a 2-D radiative-convective model using the same assumptions as Ramaswamy et al. for the vertical ozone change, specifically restricting the ozone change to be entirely in the 7 km region above the tropopause; our calculated forcing was in good agreement with that of Ramaswamy et al. Thus our radiation seems to be consistent with theirs. The reason that we obtain a larger forcing with ozone loss profile A and B is that these profiles have a substantial ozone reduction near the tropopause including a moderate loss just beneath the tropopause, while *Ramaswamy et al.* [1992], by assumption, consider only ozone loss above the tropopause. Removing a small amount of ozone from the tropopause region (where it is coldest, but ozone lines are still pressure broadened) and adding a similar amount in the lower troposphere causes a significant cooling without changing the column ozone amount.

The question is whether our estimated ozone change for the full profile exaggerates the ozone depletion and the resulting climate forcing. Observational data for ozone change, especially in the critical tropopause region, are limited and tend to change as calibrations and analyses are modified, but there is empirical evidence in observed temperature change suggesting that we have not exaggerated the forcing due to ozone depletion. The temperature change is particularly relevant, because the mechanism by which the ozone depletion cools the surface is via reduction of longwave radiation to the surface due to cooling of the local atmospheric level. The most precise relevant measure of temperature change during the period of ozone depletion is provided by microwave sounding unit (MSU) channel 4 data [*Spencer and Christy*, 1993], which samples mainly altitudes 16-24 km. The MSU data show a cooling of about 0.9°C over the period 1979-1994. Model simulations, with different radiative forcings, based on the same radiation scheme as employed here, suggest that ozone change is the main cause of the cooling, with the profile B ozone change yielding slightly less cooling than observed *[Hansen et al.*, manuscript in preparation, 1997]. This suggests that we have not exaggerated the ozone loss and the resulting lower stratospheric cooling which is the immediate cause of the negative climate forcing.

Our inference of a large negative ozone climate forcing in the period 1979-1994 is based on a rather crude estimate of the ozone change. Given the calculated magnitude of the forcing, it would be useful to obtain the best possible estimate of ozone change from all observations now available, compute the resulting climate forcing and temperature change, and compare the temperature change with observations including the profile of temperature change in the tropopause region.

7.4. Implications for Net Greenhouse Forcing

We compare our calculated radiative forcing due to observed ozone change with forcings due to well-mixed greenhouse gases in Figure 15. If profile A were correct, ozone change more than balanced all CFC forcing (and was about one third of the total greenhouse forcing). Profile B yields an even larger effect, the ozone change balancing all of the non-CO_2 greenhouse forcing (about half of the total greenhouse forcing). Of course, a balancing of global forcings does not imply a balancing of temperature changes, especially on a regional scale.

However, the bar graph presentation in Figure 15 understates the impact of stratospheric ozone depletion on the net global radiative forcing. To first order, the observed ozone change probably can be thought of as the combined effect of "stratospheric" ozone depletion, driven by anthropogenic chlorine and bromine, and a tropospheric ozone increase driven by anthropogenic pollution and biomass burning. The Cl/Br driven depletion seems likely to cause ozone depletion in the troposphere, as well as in the stratosphere, as ozone depletion in

the lower stratosphere should reduce the downward flux of stratospheric ozone. Based on either the results for the two ozone profiles in Figure 14a or on the sensitivities in Table 3, we estimate that if the Cl/Br mechanism causes a small tropospheric depletion the net forcing due to Cl/Br ozone depletion may be -0.4 to -0.5 W/m^2, which is partially balanced by a forcing of +0.1 to +0.2 W/m^2 due to the increase of tropospheric ozone caused by anthropogenic pollution. It is important to try to separate the effects on ozone of the Cl/Br and tropospheric pollution mechanisms because the Cl/Br contribution should begin to decrease in the next several years, as anthropogenic emissions of Cl and Br compounds are expected to decline.

We do not attempt to analyze the implications of the partial balancing of CFC and O_3 radiative forcings, and how this balancing will be altered by future CFC emission changes. *Daniel et al.* [1995] and *Solomon and Daniel* [1996] examine this question, assuming a negative forcing due to ozone depletion in the 1980s ranging from -0.1 W/m^2 [*Ramaswamy et al.*, 1992; *Schwarzkopf and Ramaswamy*, 1993; *IPCC*, 1994] to -0.3 W/m^2. They conclude that a surge of positive radiative forcing will occur in the first decade of the 21st century as ozone amounts recover. Our results based on observed ozone change offer support for the upper end of the effect estimated by Solomon and Daniel; that is, our results favor the stronger of their trends for net climate forcing change in the next 10 years. However, our large ozone forcing arises from just the direct ozone effect, without adding any indirect forcings.

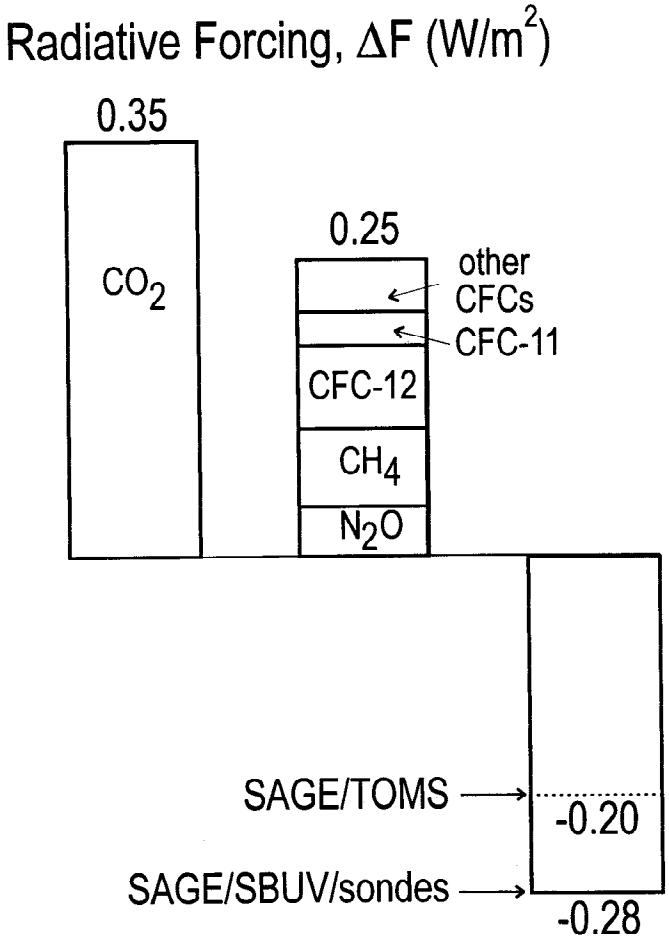

Figure 15. Adjusted radiative forcings due to measured greenhouse gas changes for the period 1979-1994. Assumed changes in abundance are ΔCO_2 = 21.5 ppm, ΔCH_4 = 162 ppb, ΔN_2O = 10.5 ppb, ΔCFC-12 = 231 ppt and ΔCFC-11 = 111 ppt. Forcing by other CFCs is based on the rate calculated by *Hansen et al.* [1989] for the 1980s, revised to account for the fact that recent data on CFC-114 and CFC-116 [*Harnisch et al.*, 1996] indicate slower growth than that assumed by *Hansen et al.* [1989]; also it is assumed that the accelerated growth of some CFCs during 1990-1994 was balanced by decelerated growth of CFC-113, the single greatest contributor to "other CFCs" in the 1980s.

Mechanisms for indirect radiative forcing due to ozone change have been proposed by *Bekki et al.* [1994] and *Toumi et al.* [1994]. Bekki et al. argue that stratospheric ozone depletion has depressed the growth rates of tropospheric CH_4 and CO, the mechanism being increased penetration of ultraviolet radiation into the troposphere and thus increased abundance of the chemical scavenger OH. Toumi et al. argue that the same mechanism increases oxidation of SO_2, thus increasing aerosol abundance and cloud albedos. There is some empirical evidence supporting slowdowns of CH_4 and CO growth during the period of increasing ozone depletion. To whatever degree the effects proposed by Bekki et al. and Toumi et al. are operating, they work in the same sense as the negative climate forcing due to ozone depletion. Evidently, quantitative evaluation of climate forcings requires more specific and accurate measurements than presently available, especially measurements of ozone, aerosol, and cloud changes.

We conclude that better measurements and understanding of ozone changes are needed to evaluate accurately present and future climate forcing, but estimates of ozone change for 1979-1994 indicate that ozone depletion in the lower stratosphere-tropopause region caused a large (negative) forcing, which considerably reduced the net greenhouse forcing of the climate system. This conclusion supports the expectation that a positive surge of net greenhouse forcing will accompany the expected recovery of lower stratospheric ozone abundance.

8. Aerosol Experiments

Both natural and anthropogenic changes of aerosols cause significant radiative forcing, as discussed in hundreds of research papers and many reviews [e.g., *Andreae*, 1995; *Charlson and Heintzenberg*, 1995; *IPCC*, 1994]. Stratospheric aerosols arising from volcanoes cause an aperiodic negative forcing, and there is evidence of global cooling after the largest eruptions [*Self and Rampino*, 1988; *Robock*, 1991; *Hansen et al.*, 1996]. Anthropogenic tropospheric aerosols are calculated to cause a cooling which may have partially balanced anthropogenic greenhouse gas warming over the past century [*Hansen et al.*, 1993a; *IPCC*, 1994; *Mitchell et al.*, 1995].

It is well recognized that the inhomogeneous distribution of aerosols implies that there can be no simple balancing of aerosol and greenhouse gas forcings. There have been many investigations of how aerosol forcing depends upon parameters such as optical depth, aerosol size, single scatter albedo, backscatter fraction or asymmetry parameter, and surface reflectivity, but the basic issue of whether the climate response has a fixed proportionality to the aerosol radiative forcing has not been studied extensively.

The fundamental aerosol parameters are optical depth τ and single scatter albedo ϖ; τ is proportional to aerosol amount; as both radiative forcing and climate response are nearly linear for

the small optical depths of greatest interest, it is sufficient in what follows to consider results for the single value $\tau = 0.1$. This leaves ϖ (which depends mainly on aerosol composition and size) as the basic parameter to be explored. All other parameters are specified implicitly via the GCM's realistic spectral and spatial distribution of surface albedos, as well as by use of an aerosol size distribution and refractive index typical of terrestrial sulfate aerosols. The effect of alternative choices for aerosol properties can be approximated well by scaling τ and ϖ with similarity relations [*van de Hulst and Grossman*, 1968; *Hansen*, 1969].

8.1. Stratospheric Aerosols

The equilibrium response in our 100-year GCM simulations with stratospheric aerosol single scatter albedo in the visible spectrum (ϖ_c) ranging from 0.8 to 1.0 is summarized in Table 9 and Figures 16a and 16b. In all cases we use a size distribution of spherical sulfuric acid aerosols with effective radius about 0.5 μm, as in the work by *Lacis et al.* [1992]. To test the effect of aerosol absorption, the sulfuric acid ϖ is replaced by ϖ_c at wavelengths where ϖ_c is less than ϖ of sulfuric acid, i.e., at essentially all wavelengths less than 3 mm.

The mean surface temperature response to the aerosol forcing in the case of conservative scattering ($\varpi_c = 1$) is consistent with that for forcings such as changes of solar irradiance, as summarized by the result $R \approx 1$ for both fixed clouds and calculated clouds. It might be anticipated that the mechanism of simple reflection of sunlight by aerosols above the troposphere has a climate effect similar to that of reduced solar irradiance, and these results confirm that expectation.

The results change dramatically for nonconservative scattering. Consider the case $\varpi_c = 0.9$: for fixed clouds the surface cooling is only -0.31°C, while for calculated clouds it is -1.75°C. The responsivity R (relative to equivalent solar forcing) is about 0.3 for fixed clouds and 1.3 for calculated clouds. A striking illustration is provided by the climate feedback factor, $f = \Delta T_s/\Delta T_0$, shown in Figures 16b and 16d: if the climate response depended only on the magnitude of the forcing, the feedback factor would be a constant $f \approx 2$-3, but we find that f varies strongly with the aerosol single scatter albedo.

This seemingly complex behavior (Figure 16 and Table 9) can be understood readily with the help of the sensitivities tabulated for "ghost" heating of different atmospheric layers (Table 4). The principal terms that must be accounted for are cooling due to the blocking of incoming solar radiation by the aerosols and heating due to absorption of solar radiation by the aerosols, which warms the stratosphere and in turn warms the surface at the rate specified by "ghost" heating. More precise analysis requires including the effect of ϖ on the amount of diffuse solar radiation and changes of absorption of upwelling radiation.

The mechanisms which cause the strong deviations of the climate response from that which would be predicted based on the adjusted forcing (or from ΔT_0) are as follows. First, for the case of fixed clouds, ΔT_s increases much more rapidly with decreasing ϖ than indicated by ΔT_0 or F_a. This is because energy absorbed in the stratosphere causes a greater warming of the surface in our GCM (and presumably in the real world) than that calculated from only radiative processes (say in a radiative-convective model). This phenomenon, demonstrated in our ghost forcing experiments (section 5), works via alteration of the lapse rate, which makes warming of the lower stratosphere more effective on surface temperature than in a radiative-convective model (Table 4, R values for fixed clouds).

Second, for the case of calculated clouds, warming of the stratosphere reduces high level (cirrus) clouds, thus causing a surface cooling which adds to the aerosol cooling, making the total feedback factor ~4. This phenomenon was isolated in our ghost forcing experiments, as quantified by the values of R less than unity for ghost heating of stratospheric layers with calculated clouds (Table 4).

Sulfuric acid, the principal stratospheric aerosol, has single scatter albedo near unity, but results for absorbing aerosols are of more than academic interest. Volcanic ash, meteoritic material, aircraft pollution, and other aerosols can have single scatter albedo significantly less than unity.

8.2. Tropospheric Aerosols

In the troposphere, absorption by aerosols has an even greater impact than it does in the stratosphere, for two reasons. First, energy absorbed within the troposphere is more effectively transferred into a T_s increase, as illustrated by the effectiveness of ghost heating vs. altitude (Figure 8 and Table 4). Second, tropospheric aerosols are concentrated in the lower layers of the atmosphere, where aerosol absorption causes a positive climate

Table 9. Stratospheric Aerosol Experiments: Radiative Forcings and Equilibrium Responses

Experiment	F_i, W/m²	F_a, W/m²	ΔT_0, °C	ΔT_s, °C		$\Delta T_s/F_a$		R	
				Fixed Clouds	All Feedbacks	Fixed Clouds	All Feedbacks	Fixed Clouds	All Feedbacks
Single scatter albedo dependence									
$\varpi = 1$	-2.84	-2.68	-0.80	-1.76	-2.63	0.66	0.98	0.98	1.00
$\varpi = 0.95$	-3.33	-2.06	-0.61	-0.95	-2.40	0.46	1.17	0.69	1.21
$\varpi = 0.90$	-3.81	-1.44	-0.43	-0.31	-1.75	0.22	1.22	0.32	1.30
$\varpi = 0.85$	-4.30	-0.83	-0.25	0.40	-1.26	-0.48	1.52	-0.72	1.66
$\varpi = 0.80$	-4.78	-0.25	-0.07	1.05	-0.76	-4.20	3.04	-6.33	3.41
Latitude dependence ($\varpi = 1$)									
Latitudes > 30°	-1.02	-0.99	-0.30	-0.70	-1.32	0.71	1.33	1.06	1.45
Latitudes < 30°	-1.83	-1.68	-0.50	-0.90	-1.20	0.54	0.71	0.80	0.76

Aerosols have optical depth 0.1, with 0.05 in each of layers 8 and 9.

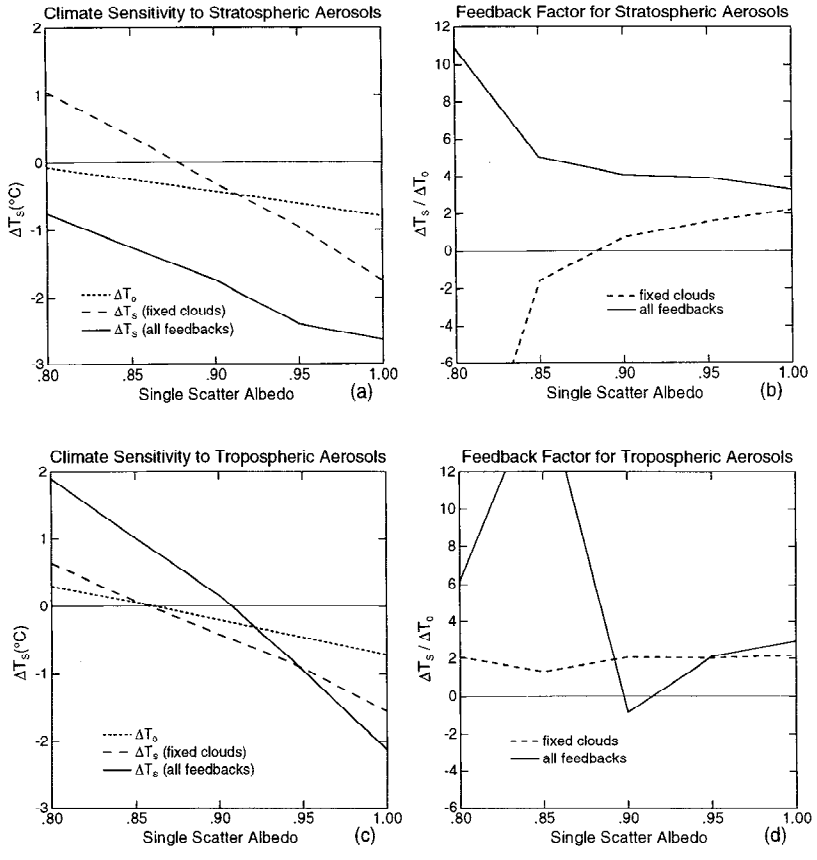

Figure 16. Surface air temperature sensitivity to a globally uniform aerosol layer of optical depth $\tau = 0.1$ located in the stratosphere with equal amounts in layers 8 and 9 (Figure 16a), and in the lowest three layers of the troposphere with approximately 1 km scale height. Figures 16b and 16d show the corresponding feedback factors as a function of aerosol single scatter albedo ϖ.

feedback by reducing local large-scale cloud cover. We refer to this effect of absorbing aerosols on clouds as the "semidirect" aerosol effect, distinguishing it from the more complex indirect aerosol effect [*Twomey*, 1974; *Charlson et al.*, 1992], which occurs via aerosols altering cloud microphysics.

Critical ϖ^*. We find that the critical single scatter albedo (ϖ^*) at which the aerosol impact on global mean surface temperature shifts from cooling to heating is $\varpi^* \approx 0.86$ for fixed clouds (Figure 16c). This is similar to the value $\varpi^* \approx 0.85$ found for a 1-D model [*Hansen et al.*, 1980], but such models by assumption exclude the semidirect aerosol effect on clouds. When this effect is included, ϖ^* increases to about 0.91 (Figure 16c).

The specific value found for ϖ^* depends on the vertical and horizontal distribution of the aerosols. The value 0.91 was obtained for a uniform global distribution of aerosols, with equal optical depths in each of the lowest three model layers; this corresponds approximately to exponential falloff with height with 1 km scale height, because layer thickness increases with height. If aerosols are instead placed higher in the atmosphere, so they tend to be above the clouds, ϖ^* is even closer to unity, as shown in Table 10 for aerosols in layers 5-6 and layers 1-7. Restricting the aerosols to occur over land, which has higher albedo than the ocean, also increases ϖ^* (Table 10; case considered by *Hansen et al.*, [1995a]). If the aerosols are given a geographical distribution representative of industrial sulfates and biomass burning, $\varpi^* \approx 0.87$ (Table 10; case considered by Hansen *et al.*, 1993a), being reduced by the large effect of smoke aerosols over low-albedo ocean areas.

These values of ϖ^* are sufficiently large to call into question at least the magnitude and perhaps the sign of the direct anthropogenic aerosol effect on T_s, even though the aerosol forcing is almost certainly negative. The reason is that $\varpi^* = 0.9$ is not much less than the values estimated for the single scatter albedo of the principal anthropogenic aerosols, including aerosols from fossil fuel combustion, biomass burning [*Penner et al.*, 1992], and disturbed desert dust [*Tegen et al.*, 1996].

The sensitivity of ΔT_s to aerosol absorption is well recognized [e.g., *Chylek and Wong*, 1995; *Haywood and Shine*, 1995]. Quantitative evaluation requires knowledge of the aerosol size distribution [*Kiehl and Briegleb*, 1993]; [*Chylek et al.*, 1995] because the backscatter fraction depends on aerosol size. Results for different size distributions can be estimated from our results, which are for a specific size distribution ($r_{eff} = 0.5$ and asymmetry parameter is 0.7) of sulfuric acid aerosols, by use of appropriate scaling relations, as mentioned above, but it would be necessary to have knowledge of particle sizes globally to evaluate aerosol climate forcing and response.

Our aim here is not an evaluation of global heating or cooling by aerosols. Rather our purpose is to point out that (1) the fixed proportionality between ΔT_s and F_a (and thus the fixed climate feedback factor, $\Delta T_s/\Delta T_0$) that holds approximately for changes

Table 10. Tropospheric Aerosol ($\Delta\tau = 0.1$) Experiments: Radiative Forcings and Equilibrium Responses

Experiment	F_i, W/m²	F_a, W/m²	ΔT_0, °C	ΔT_s, °C		$\Delta T_s/F_a$		R	
				Fixed Clouds	All Feedbacks	Fixed Clouds	All Feedbacks	Fixed Clouds	All Feedbacks
Single scattering albedo dependence (layers 1-3)									
$\varpi = 1$	-2.44	-2.43	-0.72	-1.55	-2.12	0.64	0.87	0.95	0.90
$\varpi = 0.95$	-1.62	-1.61	-0.45	-0.91	-0.94	0.57	0.58	0.84	0.62
$\varpi = 0.90$	-0.82	-0.82	-0.20	-0.41	0.17	0.50	-0.21	0.75	-0.23
$\varpi = 0.85$	-0.03	-0.03	0.06	0.08	1.01	-2.67	-33.70	-4.00	-37.40
$\varpi = 0.80$	0.75	0.74	0.31	0.64	1.90	0.86	2.57	1.31	3.00
Height dependence									
Layers 1-3, $\varpi = 1$	-2.44	-2.43	-0.72	-1.55	-2.12	0.64	0.87	0.95	0.90
Layers 5-6, $\varpi = 1$	-2.23	-2.23	-0.65	-1.40	-1.91	0.63	0.86	0.94	0.89
Layers 1-3, $\varpi = 0.9$	-0.82	-0.82	-0.20	-0.41	0.17	0.50	-0.21	0.75	-0.23
Layers 1-7, $\varpi = 0.9$	0.20	0.24	0.12	0.03	-0.57	0.13	-2.38	0.19	-2.71
Layers 5-6, $\varpi = 0.9$	0.89	0.84	0.30	0.11	-0.76	0.13	-0.90	0.20	-1.06
Spatial distribution dependence (layers 1-3)									
$\varpi = 1$									
Global, $\Delta\tau = 0.1$	-2.44	-2.43	-0.72	-1.55	-2.12	0.64	0.87	0.95	0.90
Land, $\Delta\tau = 1/3$	-1.84	-1.83	-0.55	-1.09	-1.20	0.60	0.66	0.89	0.69
R&E, $\Delta\tau_{globe} = 0.034$	-0.85	-0.86	-0.25	-0.51	-0.78	0.59	0.91	0.89	0.99
$\varpi = 0.9$									
Global, $\Delta\tau = 0.1$	-0.82	-0.82	-0.20	-0.41	0.17	0.50	-0.21	0.75	-0.23
Land, $\Delta\tau = 1/3$	-0.02	-0.02	0.03	0.09	0.55	-4.50	-27.50	-6.92	-30.60
R&E, $\Delta\tau_{globe} = 0.034$	-0.32	-0.32	-0.09	-0.21	-0.16	0.66	0.50	0.99	0.56
R&E aerosols (sulfate + smoke, $\tau = 0.034$) + GHG									
$\varpi = 1.0$	0.07	0.00	0.00	0.01	0.27	-	∞	-	∞
$\varpi = 0.9$	0.03	0.00	0.00	-0.01	0.26	-	∞	-	∞

R&E refers to paper by *Hansen et al.* (1993a) in *Research and Exploration.*

of CO_2, solar irradiance and some other forcings is not accurate for absorbing aerosols, and (2) when our simulation of the semidirect aerosol effect on clouds is included with $\varpi \approx 0.9$-0.95, the surface temperature change is very small. Furthermore, values of $\varpi \approx 0.9$ are not hypothetical. *Ogren and Sheridan* [1996] report values typically $\varpi \approx 0.88$-0.96 for aircraft measurements of tropospheric aerosols over the United States. *Penner et al.*[1992] estimate $\varpi \approx 0.92$ for biomass burning aerosols. Mie calculations by *Haywood and Shine* [1995] for plausible soot/sulfate aerosol composition yield typically $\varpi \approx 0.8$-0.96. The extensive aerosols from disturbed soils in arid regions typically have $\varpi \approx 0.85$-0.95 (Tegen *et al.*, 1996).

Aerosols versus greenhouse gases. We examine the difference in the climate response to aerosol and greenhouse gas forcings by considering two cases in which the aerosol and greenhouse gas forcings are equal in magnitude and opposite in sign. In the first case we use aerosol single scattering albedo $\varpi = 1$ and in the second case $\varpi = 0.9$. In both cases we use the geographical distribution of aerosols specified in Figure 16 of *Hansen et al.* [1993a]. The global mean aerosol optical depth is $\tau = 0.034$, with 0.017 distributed according to the sulfate distribution of *Charlson et al.* [1991] and the other 0.017 distributed at low latitudes simulating biomass burning. Adjusted forcings are ≈ -0.86 W/m² for $\varpi = 1$ and ≈ -0.32 W/m² for $\varpi = 0.9$. The amount of greenhouse gases was taken as that occurring at the time in the greenhouse gas scenario of *Hansen et al.* [1993a] at which the adjusted greenhouse gas forcing exactly balanced the adjusted aerosol forcing. Results for the calculated climate response are summarized in Table 10 and Plates 8 and 9.

The global mean ΔT_s is small for both $\varpi = 1$ and $\varpi = 0.9$ in the case of fixed clouds. Also the regional response (ΔT_s) is damped and smoothed considerably, relative to the forcing (F_a), although some hint of the location of the forcings is maintained in the response. On the other hand, with calculated clouds there is a large global mean warming for both $\varpi = 1$ and $\varpi = 0.9$. For the case $\varpi = 1$ this arises because there is a strong net positive forcing in the sea ice regions which have high equilibrium sensitivity in our model. For the case $\varpi = 0.9$ the mechanism causing the global warming is the semidirect effect of absorbing aerosols on low level cloud cover.

Summary. Our general conclusion is that in comparing aerosol and greenhouse gas climate effects, it can be misleading and is thus insufficient to simply compare their radiative

forcings. Our specific conclusion regarding anthropogenic aerosols is that their net "direct" impact on global surface temperature, including "semidirect" changes of cloud cover, is probably small and even its sign is uncertain.

These conclusions do not refer to the indirect aerosol effect on cloud microphysics [*Twomey*, 1974; *Charlson et al.*, 1992; *IPCC*, 1994] which is believed to cause a significant negative climate forcing. Indeed, observations of cooling in regions of anthropogenic aerosols [*Karl et al.*, 1995] and damping of the diurnal cycle over land areas [*Hansen et al.*, 1995a] offer empirical evidence for such an indirect aerosol effect. Rather our results call into question the conclusion [*Charlson et al.*, 1992; *IPCC*, 1994] that the direct aerosol effect has an impact on global temperature comparable to the indirect aerosol effect, with both causing cooling represented by a forcing of the order of 1 W/m^2. Other recent studies [*Kiehl and Briegleb*, 1993; *Hansen et al.*, 1993a] have suggested that the magnitude of the direct aerosol forcing was being overestimated, as reflected in *IPCC* [1995]; the present results carry this one step further, suggesting that anthropogenic aerosols have little if any direct cooling effect.

9. Surface Albedo Experiments

Surface albedo changes are another important climate forcing. Changes in ice sheet area and vegetation distribution are estimated to have caused a forcing -3.5 W/m^2 during the ice age 20,000 years ago, about half of the forcing required to maintain the ice age cold [*Hansen et al.*, 1993a]. A surface albedo change of more immediate interest is that caused by anthropogenic land use. Hansen et al. (manuscript in preparation, 1997) calculate a global mean forcing of -0.4 W/m^2 when natural (preindustrial) vegetation is replaced by current land use patterns. Thus it is of interest to determine the effectiveness of surface albedo forcings.

In our first surface albedo experiment we increased the surface albedo by 0.2 over all of Tropicana, and in a second experiment we increased the albedo of Northland by 0.2 at latitudes $\leq$ 55°N. The results (Table 11) show that albedo change is somewhat less effective than an equivalent change of solar irradiance ($R < 1$), especially in the case of calculated clouds. This result might seem surprising, given the similar nature of the forcing for an albedo change and a solar irradiance change, but the forcings differ because the surface albedo change occurs at a specific range of latitudes, while the solar forcing has a smooth distribution with latitude, peaking at the equator (Figure 4). The present results are consistent with the latitude dependence of the responsivity to a ghost forcing into the surface (Table 4), which was discussed in section 5. For example, the low responsivity with calculated clouds is in part a result of the forcing being confined to northern hemisphere latitudes, where it does not excite the strong southern hemisphere sea ice feedback (Table 4).

We conclude that surface albedo change is a reasonably well-behaved forcing. However, its effectiveness is a function of the geographic location of the albedo change.

Finally, it is of interest to ask whether a surface albedo change is equivalent to an aerosol forcing of equal value. *Mitchell et al.* [1995] implicitly make that assumption in their GCM simulations, as for convenience they use albedo change as a proxy for aerosol change. Although we have not made calculations of those forcings applied to the same region, our results suggest that the substitution is not a bad approximation for the case of conservatively scattering aerosols ($\varpi = 1$). However, based on results in section 8.2, it is not in general a good approximation for aerosols with absorptions typical of the real world.

10. Discussion

Radiative forcing is an invaluable tool for analysis of climate change. We have found that the magnitude of the forcing is a fairly accurate predictor of the climate response in our GCM for most globally distributed radiative forcings, provided that the forcing is calculated after the stratospheric temperature has adjusted to the perturbation. However, there is a sensitivity of the climate response to the altitude and latitude of the forcing, which can alter the response/forcing ratio by several tens of percent or more in particular cases. Thus precise climate change studies must take into consideration the nature of the climate forcing as well as its magnitude in watts per square meter.

The principal mechanisms causing the climate responsivity to vary from one forcing to another can be understood readily. One mechanism involves the tropospheric lapse rate, which can be altered depending upon the atmospheric level at which the radiative forcing is applied. A forcing in the upper troposphere, for example, preferentially warms or cools those layers, which adjust in part via radiation to space rather than by causing a temperature change uniformly through the column.

A second mechanism causing the climate responsivity to vary from one forcing to another is the change of cloud cover caused by the forcing. The principal effect of heating within a given atmospheric layer is to reduce large-scale clouds within that layer. A specific case in which this mechanism may be important is absorbing tropospheric aerosols. We describe this aerosol impact on clouds as a "semidirect" aerosol cloud effect. Its effect on cloud cover and surface temperature tends to be of opposite sign (warming) and thus compete with cooling from the so-called indirect aerosol-cloud effect.

The precision with which these mechanisms are represented is dependent upon the degree of realism in our global climate model, which is limited by the use of the physical representations in the primitive GCM of *Hansen et al.* [1983]. Although the existence and sense of these mechanisms appear to be

Table 11. Surface Albedo Experiments: Radiative Forcings and Equilibrium Responses

Experiment	F_i, W/m^2	F_a, W/m^2	ΔT_0, °C	ΔT_s,°C		$\Delta T_s/F_a$		R	
				Fixed Clouds	All Feedbacks	Fixed Clouds	All Feedbacks	Fixed Clouds	All Feedbacks
+20% over land									
Tropicana	-3.72	-3.70	-1.08	-2.21	-1.59	0.60	0.43	0.88	0.42
Northland (lat$\leq$55°N)	-2.16	-2.15	-0.69	-1.33	-1.39	0.62	0.65	0.92	0.67

straightforward, their magnitude depends on features of our particular model, especially the calculated clouds, and thus the mechanisms should be studied with other global models. However, we do not expect our overall conclusion, that climate response depends on the nature of the forcing as well as its magnitude, to be altered. We find that the results in recent papers touching on this topic, i.e., the dependence of climate response on the nature of the forcing, are in excellent agreement with the quantitative results in our tables. For example, we obtain the same small sensitivity to forcings found by *Chen and Ramaswamy* [1996] for cloud microphysical changes when they are restricted to the same level, latitudes, and fixed cloud cover as in the Chen and Ramaswamy experiments.

We note that the broad range of climate mechanisms and forcings investigated in our present study serves to illustrate the merits of a highly efficient GCM for climate studies, as discussed in paper W1. Realistic simulation of climate mechanisms depends upon unconstrained coupling of the fundamental equations describing the system, as is permitted in a three-dimensional GCM, but it also requires a model with an efficiency permitting multiple experiments with different parameter values.

Our present experiments yield, in addition to the above general conclusions, information on several specific climate forcings. We summarize here results for three of these forcings.

Ozone change. At face value, observed values of ozone change during the period (1979-1994) imply a large negative radiative forcing, which offsets most of the positive forcing due to increasing carbon dioxide. The forcing due to ozone change is uncertain because it depends particularly on ozone changes in the middle and upper troposphere, where there are few measurements, especially at low latitudes. Unless the ozone changes are determined more precisely, it will be difficult to interpret quantitatively observed climate change. Nevertheless, available ozone data suggest that ozone change was a strong negative forcing over the past 1 1/2 decades. The calculations support the contention that the net greenhouse gas climate forcing will increase more rapidly in the near future as global ozone recovers from current anthropogenic depletion.

Tropospheric aerosols. Absorbing tropospheric aerosols are a case in which the fixed proportionality between radiative forcing and climate response can break down. Aerosols with single scatter albedos as large as $\varpi \approx 0.9$ can lead to net global warming, in part because of a semidirect cloud effect which reduces large-scale cloud cover in layers with absorbing aerosols. Present aerosol measurements are inadequate for a global assessment, but limited available data suggest that on average anthropogenic aerosols are probably in the range $\varpi = 0.9$-0.95. If so, the mean effect of aerosols on surface temperature is nearly neutral, excluding their indirect effect on cloud microphysics, and their overall effect is less of a negative forcing than has commonly been assumed.

Solar irradiance. The net radiative forcing due to solar cycle irradiance variations and associated atmospheric ozone changes is about 0.2 W/m^2. This is sufficient to yield a climate response that is probably detectable, but of little practical significance. The climate response to solar variations on the timescale of the solar cycle is practically insensitive to uncertainties in equilibrium climate sensitivity, i.e., to the magnitude of radiative feedbacks. We conclude that it is not possible to infer climate sensitivity from observed cyclic variability of surface air temperature on decadal timescales. Solar variability may have more important climate effects on longer time scales, as the irradiance changes may be larger and the climate system has time to respond more fully.

These findings have relevance to the interpretation of global climate change and assessment of the possible role of humankind in altering climate. The overall conclusion that radiative forcings are usually a good predictor of equilibrium climate response, and that exceptions are understandable and can be appropriately accounted for, is an optimistic one for climate interpretation and assessment, but the sensitivity of the net global forcing to ozone changes in the middle and upper troposphere and even more the sensitivity to small amounts of aerosol absorption and associated changes in cloud cover imply that present global measurements are inadequate for reliable interpretation of long-term climate change [*Hansen et al.*, 1993b].

Acknowledgments. We are especially indebted to Andy Lacis, who developed the powerful radiative transfer algorithms in the GISS climate model and spent many hours schooling us in their proper use. Stacey Hollandsworth, Jennifer Logan, Joe Zawodny, and Rich McPeters provided ozone data and Judith Lean provided solar irradiance data; the data are used here as well as in the more realistic experiments of J. Hansen et al. (manuscript in preparation, 1997). Keith Shine and V. Ramaswamy provided useful comments on our draft manuscript. Jeff Jonas, Lilly Del Valle, and Jose Mendoza helped with graphics, Christina Koizumi helped with graphics and desktop publishing, and Ely Duenas helped with desktop publishing. This work was supported by the NASA Climate, EOS, and Aircraft Assessment programs.

References

Andreae, M.O., Climatic effects of changing atmospheric aerosol levels, in *World Survey of Climatology*, vol. 16, *Future Climates of the World*, edited by A. Henderson-Sellers, pp. 341-392, Elsevier, New York, 1995.

Bekki, S., K.S. Law, and J.A. Pyle, Effect of ozone depletion on atmospheric CH_4 and CO concentrations, *Nature, 371,* 595-597, 1994.

Blake, D.F., and K. Kato, Latitudinal distribution of black carbon soot in the upper troposphere and lower stratosphere, *J. Geophys. Res., 100,* 100, 7195-7202, 1995.

Cess, R.D., et al., Uncertainties in CO_2 radiative forcing in atmospheric general circulation models, *Science, 262,* 1252-1255, 1993.

Charlson, R.J., and J. Heintzenberg, *Aerosol Forcing of Climate*, 416 pp., John Wiley, New York, 1995.

Charlson, R.J., J. Langner, H. Rodhe, C.B. Leovy, and S.G. Warren, Perturbation of the northern hemisphere radiative balance by backscattering from anthropogenic sulfate aerosols, *Tellus,Ser. B, 43,* 152-163, 1991.

Charlson, R.J., S.E. Schwartz, J.M. Hales, R.D. Cess, J.A. Coakley, J.E. Hansen, and D.J. Hofmann, Climate forcing by atmospheric aerosols, *Science, 255,* 423-430, 1992.

Chen, C.T., and V. Ramaswamy, Sensitivity of simulated global climate to perturbations in low-cloud microphysical properties, I, Globally uniform perturbations, *J. Clim., 9,* 1385-1402, 1996.

Chylek, P., and J. Wong, Effect of absorbing aerosols on global radiation budget, *Geophys. Res. Lett., 22,* 929-931, 1995.

Chylek, P., G. Videen, D. Ngo, R.G. Pinnick, and J.D. Klett, Effect of black carbon on the optical properties and climate forcing of sulfate aerosols, *J. Geophys. Res., 100,* 16, 325, 332, 1995.

Cunnold, D.M., H. Wang, W.P. Chu, and L. Froidevaux, Comparisons between Stratospheric Aerosol and Gas Experiment II and microwave limb sounder ozone

measurements and aliasing of SAGE II ozone trends in the lower stratosphere, *J. Geophys. Res., 101,* 10, 061-10, 075, 1996.

Currie, R.G., Solar cycle signal in air temperature in North America: Amplitude, gradient, phase and distribution, *J. Atmos. Sci., 38,* 808-818, 1981.

Daniel, J.S., S. Solomon, and D.L. Albritton, On the evaluation of halocarbon radiative forcing and global warming potentials, *J. Geophys. Res., 100,* 1271-1285, 1995.

Hansen, J.E., Absorption line formation in a planetary atmosphere: A test of van de Hulst's similarity relations, *Astrophys. J., 158,* 337-349, 1969.

Hansen, J.E., and A.A. Lacis, Sun and dust versus greenhouse gases: An assessment of their relative roles in global climate change, *Nature, 346,* 713-719, 1990.

Hansen, J., and S. Lebedeff, Global trends of measured surface air temperature, *J. Geophys. Res., 92,* 13,345-13,372, 1987.

Hansen, J.E., A.A. Lacis, P. Lee, and W.C. Wang, Climatic effects of atmospheric aerosols, *Ann. N. Y. Acad. Sci., 338,* 575-587, 1980.

Hansen, J., G. Russell, D. Rind, P. Stone, A. Lacis, S. Lebedeff, R. Ruedy, and L. Travis, Efficient three- dimensional global climate models for climate studies: models I and II, *Mon. Weather. Rev., 111,* 609-662, 1983.

Hansen, J., A. Lacis, D. Rind, G. Russell, P. Stone, I. Fung, R. Ruedy and J. Lerner, Climate sensitivity: Analysis of feedback mechanisms, in *Climate Processes and Climate Sensitivity, Geophys. Monogr. Ser.*, vol. 29, edited by J. E. Hansen and T. Takahashi, pp. 130-163, *AGU,* Washington, D.C., 1984.

Hansen, J., G. Russell, A. Lacis, I. Fung, D. Rind, and P. Stone, Climate response times: dependence on climate sensitivity and ocean mixing, *Science, 229,* 857-859, 1985.

Hansen, J., I. Fung, A. Lacis, D. Rind, S. Lebedeff, R. Ruedy, G. Russell, and P. Stone, Global climate changes as forecast by Goddard Institute for Space Studies three-dimensional model, *J. Geophys. Res., 93,* 9341-9364, 1988.

Hansen, J., A. Lacis, and M. Prather, Greenhouse effect of chlorofluorocarbons and other trace gases, *J. Geophys. Res., 94,* 16,417-16,421, 1989.

Hansen, J., A. Lacis, R. Ruedy, M. Sato, and H. Wilson, How sensitive is the world's climate?, *Natl. Geogr. Res. Explor., 9,* 142-158, 1993a.

Hansen, J., W. Rossow, and I. Fung, Long-term monitoring of global climate forcings and feedbacks, *NASA Conf. Publ., CP 3234,* in *Proceedings of Workshop held at Goddard Institute for Space Studies, New York, February 3-4, 1992*, 26-35, 1993b.

Hansen, J., M. Sato, A. Lacis, and R. Ruedy, Climatic impact of ozone change, in *The Impact on Climate of Ozone Change and Aerosols, Background Material from the Joint Workshop of IPCC Working Group I and the International Ozone Assessment Panel,* pp. 18-26, World Meteorol. Org., Geneva 1993c.

Hansen, J., M. Sato, and R. Ruedy, Long-term changes of the diurnal temperature cycle: implications about mechanisms of global climate change, *Atmos. Res., 37,* 175-209, 1995a.

Hansen, J., H. Wilson, M. Sato, R. Ruedy, K. Shah, and E. Hansen, Satellite and surface temperature data at odds?, *Clim. Change, 30,* 103-117, 1995b.

Hansen, J., et al., A Pinatubo climate modeling investigation, *Global Environment Change, NATO ASI Ser., Ser. I,* edited by G. Fiocco, D. Fua', and G. Visconti, pp. 233-272, Springer-Verlag, New York, 1996.

Hansen, J., R. Ruedy, A. Lacis, G. Russell, M. Sato, J. Lerner, D. Rind, and P. Stone, Wonderland climate model, *J. Geophys. Res.*, this issue.

Harnisch, J. R. Borchers, P. Fabian, and M. Maiss, Tropospheric trends for CF_4 and C_2F_2 since 1982 derived from SF_6 dated stratospheric air, *Geophys. Res. Lett., 23,* 1099-1102, 1996.

Hauglustaine, D.A., C. Granier, G.P. Brasseur, and G. Megie, The importance of atmospheric chemistry in the calculation of radiative forcing of the climate system, *J. Geophys. Res., 99,* 1173-1186, 1994.

Haywood, J.M., and K.P. Shine, The effect of anthropogenic sulfate and soot aerosol on the clear sky planetary radiation budget, *Geophys. Res. Lett., 22,* 603-606, 1995.

Hickey, J.R., B.M.Alton, H.L. Kyle, and D. Hoyt, Total solar irradiance measurements by ERB/Nimbus 7: A review of nine years, *Space Sci. Rev.*,321-342, 1988.

Hollandsworth, S.M., R.D. McPeters, L.E. Flynn, W. Planet, A.J. Miller, and S. Chandra, Ozone trends deduced from combined Nimbus 7 SBUV and NOAA 11 SBUV/2 data, *Geophys. Res. Lett., 22,* 905-908, 1995.

Intergovernmental Panel on Climate Change, *Climate Change, The IPCC Scientific Assessment*, edited by J.T. Houghton, C.J. Jenkins, and J.J. Ephraums, 200 pp., Cambridge Univ. Press, New York, 1990.

Intergovernmental Panel on Climate Change, *Climate Change 1992, The Supplementary Report to the IPCC Scientific Assessment*, edited by J.T. Houghton, B.A. Callander, and S.K. Varney, 200 pp., Cambridge Univ. Press, New York, 1992.

Intergovernmental Panel on Climate Change, *Climate Change: Radiative Forcing of Climate Change: The Scientific Assessment*, 339 pp., Cambridge Univ. Press, New York, 1994.

Intergovernmental Panel on Climate Change, *Climate Change 1995: The Science of Climate Change,* 572 pp., Cambridge Univ. Press, New York, 1995.

Jiang, Y., and Y. L. Yung, Concentrations of tropospheric ozone from 1979 to 1992 over tropical Pacific South America from TOMS data, *Science, 272,* 714-716, 1996.

Karl, T.R., R.W. Knight, G. Kukla, and G. Gavin, Evidence for the radiative effects of anthropogenic sulfate aerosols in the observed climate record, in *Aerosol Forcing of Climate*, edited by R. Charlson and J. Heintzenberg, pp. 363-382, John Wiley, New York, 1995.

Kawa, S.R., R.A. Plumb, and U. Schmidt, Simultaneous observations of long-lived species, in *The Atmospheric Effects of Stratospheric Aircraft,* vol III, edited by M.J. Prather and E.E. Remsberg, *NASA Ref. Publ.1292*, NASA MTPE, Washington, 352 pp., H1-H49, 1993.

Kiehl, J.T., and B.P. Briegleb, The relative roles of sulfate aerosol and greenhouse gases in climate forcing, *Science, 260,* 311-314, 1993.

Lacis, A.A., and V. Oinas, A description of the correlated *k* distribution method for modeling nongray gaseous absorption, thermal emission, and multiple scattering in vertically inhomogeneous atmospheres, *J. Geophys. Res., 96,* 9027-9063, 1991.

Lacis, A.A., W.C. Wang, and J.E. Hansen, Correlated k-distribution method for radiative transfer in climate models: Application to effect of cirrus clouds on climate, in *NASA*

Weather and Climate Science Review, NASA Conf. Publ., CP 2076, 309-314, 1979.

Lacis, A.A., D.J. Wuebbles, and J.A. Logan, Radiative forcing of climate by changes of the vertical distribution of ozone, *J. Geophys. Res., 95*, 9971-9981, 1990.

Lacis, A., J. Hansen, and M. Sato, Climate forcing by stratospheric aerosols, *Geophys. Res. Lett., 19*, 1607-1610, 1992.

Lean, J., Variations in the Sun's radiative output, *Rev. Geophys., 29*, 505-535, 1991.

Lean, J.L., O.R. White, and A. Skumanich, On the solar ultraviolet spectral irradiance during the Maunder Minimum, *Global Biogeochem. Cycles, 9*, 171-182, 1995.

Li, Z., and P. Varanasi, Measurements of the absorption cross-sections of CFC-11 at conditions representing various model atmospheres, *J. Quant. Spectrosc. Radiat. Transfer, 52*, 137-144, 1994.

Logan, J.A., Trends in the vertical distribution of ozone: An analysis of ozonesonde data, *J. Geophys. Res., 99*, 25, 553-25, 585, 1994.

Manabe, S., Cloudiness and the radiative, convective equilibrium, in *The Changing Global Environment*, edited by S.F. Singer, pp. 175-176, D. Reidel, Norwell, Mass., 1975.

Manabe, S., and R.F. Strickler, Thermal equilibrium of the atmosphere with a convective adjustment, *J. Atmos. Sci., 21*, 361-385, 1964.

Manabe, S., and R.T. Wetherald, The effects of doubling the CO_2 concentration on the climate of a general circulation model, *J. Atmos. Sci., 32*, 3-15, 1975.

Manabe, S., K. Bryan, and M.J. Spelman, Transient response of a global ocean-atmosphere model to a doubling of atmospheric carbon dioxide, *J. Phys. Oceanogr., 20*, 722- 749, 1990.

McCormick, M.P., R.E. Veiga, and W.P. Chu, Stratospheric ozone profile and total ozone trends derived from the SAGE I and SAGE II data, *Geophys. Res. Lett., 19*, 269-272, 1992.

McPeters, R.D., Ozone profile comparisons, in *The Atmospheric Effects of Stratospheric Aircraft*, vol. II, edited by M.J. Prather and E.E. Remsberg, *NASA Ref. Publ. 1292*, D1-D37, 1993.

Mitchell, J.F.B., R.A. Davis, W.J. Ingram, and C.A. Senior, On surface temperature, greenhouse gases, and aerosols: Models and observations, *J. Clim., 8*, 2364-2386, 1995.

Morcillo, J., L.J. Zamorano, and J.M.V. Heredia, Infra-red intensities in CH_2F_2, CH_2Cl_2 and CF_2Cl_2, *Spectrochim. Acta, 22*, 1969-1980, 1966.

Nanes, R., P.M. Silvaggio, and R.W. Boese, Temperature dependence of intensities of the 8-12 μm bands of $CFCl_3$, *J. Quant. Spectrosc. Radiat. Transfer, 23*, 211-230, 1980.

Nightingale, R.W., et al., Global CF2Cl2 measurements by UARS cryogenic limb array etalon spectrometer: Validation by correlative data and a model, *J. Geophys. Res., 101*, 9711-9736, 1996.

Ogren, J.A., and P.J. Sheridan, Vertical and horizontal variability of aerosol single scattering albedo and hemispheric backscatter fraction over the United States, paper presented at Conference on Nucleation and Atmospheric Aerosols, University of Helsinki, Helsinki, Finland, Aug. 26-30, 780-783, 1996.

Penner, J.E., R.E. Dickinson, and C.A. O'Neill, Effects of aerosol from biomass burning on the global radiation budget, *Science, 256*, 1432-1434, 1992.

Person, W.B., S.K. Rudys, and J.H. Newton, Absolute integrated infrared absorption intensities of $CFCl_3$ and CF_3I fundamentals in the gas phase. An intensity sum rule, *J. Phys. Chem., 79*, 2525-2531, 1975.

Pinnock, S., M.D. Hurley, K.P. Shine, T.J. Wallington, and T.J. Smyth, Radiative forcing of climate by hydrochlorofluorocarbons and hydrofluorocarbons, *J. Geophys. Res., 100*, 23,227-23,238, 1995.

Ramaswamy, V., M.D. Schwarzkopf, and K.P. Shine, Radiative forcing of climate from halocarbon-induced global stratospheric ozone loss, *Nature, 355*, 810-812, 1992.

Rind, D., and P. Lonergan, Modeled impacts of stratospheric ozone and water vapor perturbations with implications for high-speed civil transport aircraft, *J. Geophys. Res., 100*, 7381-7396, 1995.

Robock, A., The volcanic contribution to climate change of the past 100 years, in *Greenhouse-Gas-Induced Climatic Change: A Critical Evaluation of Simulations and Observations*, edited by M.E. Schlesinger, pp. 429-443, Elsevier, New York, 1991.

Russell, G.L., J.R. Miller, and L.C. Tsang, Seasonal oceanic heat transports computed from an atmospheric model, *Dyn. Atmos. Oceans, 9*, 253-271, 1985.

Schwarzkopf, M.D., and V. Ramaswamy, Radiative forcing due to ozone in the 1980s: Dependence on altitude of ozone change, *Geophys. Res. Lett., 20*, 205-208, 1993.

Self, S., and M.R. Rampino, The relationship between volcanic eruptions and climate change: Still a conundrum?, *Eos, Trans. AGU, 69*, 74-75, 85-86, 1988.

Solomon, S., and J.S. Daniel, Impact of the Montreal protocol and its amendments on the rate of change of global radiative forcing, *Clim. Change, 32*, 7-17, 1996.

Spencer, R.W., and J.R. Christy, Precision lower stratospheric temperature monitoring with the MSU: Technique, validation, and results 1979-1991, *J. Clim., 6*, 1194-1204, 1993.

Stephens, G.L., and P.J. Webster, Clouds and climate: Sensitivity of simple systems, *J. Atmos. Sci., 38*, 235-247, 1981.

Stevens, M.J., and G.R. North, Using the solar cycle to estimate climate sensitivity, *J. Atmos. Sci., 53*, 2594-2608, 1996.

Stolarski, R.S., P. Bloomfield, R.D. McPeters, and J.R. Herman, Total ozone trends deduced from Nimbus 7 TOMS data, *Geophys. Res. Lett., 18*, 1015-1018, 1991.

Tegen, I., A.A. Lacis, and I. Fung, The influence of mineral aerosols from disturbed soils on climate forcing, *Nature, 380*, 419-422, 1996.

Toumi, R., S. Bekki, and K.S. Law, Indirect influence of ozone depletion on climate forcing by clouds, *Nature, 372*,348-351, 1994.

Twomey, S., Pollution and the planetary albedo, *Atmos. Environ., 8*, 1251-1256, 1974.

van de Hulst, H.C., and K. Grossman, Multiple light scattering in planetary atmospheres, in *The Atmospheres of Mars and Venus*, edited by J.C. Brandt and M.B. McElroy, pp. 35-55, Gordon and Breach, New York, 1968.

Wang, H.J., D.M. Cunnold, and X. Bao, a critical analysis of Stratospheric Aerosol and Gas Experiment ozone trends, *J. Geophys. Res., 101*, 12,495-12,514, 1996.

Wang, W.C., M.P. Dudek, X.Z. Liang, and J.T. Kiehl, Inadequacy of effective CO_2 as a proxy in simulating the greenhouse effect of other radiatively active gases, *Nature, 350*, 573-577, 1991.

Wetherald, R.T., and S. Manabe, The effects of changing the

solar constant on the climate of a general circulation model, *J. Atmos. Sci., 32,* 2044-2059, 1975.

Willson, R.C., Irradiance observations of SMM, Spacelab 1, UARS and ATLAS ACRIM experiments, in *The Sun as a Variable Star: Solar and Stellar Irradiance Variations,* edited by J. Pap, C. Frohlich, H. Hudson, and S. Solanki, pp. 54-62, Cambridge Univ. Press, New York, 1994.

Willson, R.C., and H.S. Hudson, The Sun's luminosity over a complete solar cycle, *Nature, 351,* 42-44, 1991.

World Meteorological Organization, Scientific assessment of ozone depletion, *Global Ozone Res. Monit. Rep. 16,* Geneva, 1992.

J. Hansen, R. Ruedy, and M. Sato, NASA Goddard Institute for Space Studies, 2880 Broadway, New York, NY 10025. (e-mail: jhansen@giss.nasa.gov; rruedy@giss.nasa.gov; makis@giss.nasa.gov)

(Received July 8, 1996; revised October 29, 1996; accepted October 29, 1996.)